SMAD2 sets divergent thresholds for TGF-β-induced SMAD1/5 signaling and IgE-mediated pro-inflammatory activation in mast cells

Gina Bronneberg[1], Steffen K. Meurer[2], Marlies Kauffmann[1], Chao-Chung Kuo[3], Christian Liedtke[4], Ralf Weiskirchen[2], and Michael Huber[1]*

Affiliations

[1] Institute of Biochemistry and Molecular Immunology, Medical Faculty, RWTH Aachen University, 52074 Aachen, Germany

[2] Institute of Molecular Pathobiochemistry, Experimental Gene Therapy and Clinical Chemistry (IFMPEGKC), Medical Faculty, RWTH Aachen University, 52074 Aachen, Germany

[3] Genomics Facility, IZKF Aachen, RWTH Aachen University, 52074 Aachen, Germany

[4] Department of Internal Medicine III, Medical Faculty, RWTH Aachen University, 52074 Aachen, Germany

* corresponding author

Institute of Biochemistry and Molecular Immunology, Medical Faculty, RWTH Aachen University, Pauwelsstraße 30, 52074 Aachen, Germany

E-mail: mhuber@ukaachen.de

Abstract

TGF-β-mediated signaling controls mast cell (MC) development and exerts anti-inflammatory functions, while antigen/allergen (Ag)-triggered FcεRI activation commands pro-inflammatory reactions. TGF-β induces strong C-terminal and low linker phosphorylation of SMAD2. In contrast, Ag triggers immediate, MEK-dependent SMAD2 linker phosphorylation only. Both stimuli can positively or negatively influence each other's effects on MC activation in a gene-dependent manner. However, the molecular and cellular mechanisms of SMAD2 in MCs still need to be elucidated. To decipher the role(s) of SMAD2 in MCs, SMAD2 was ablated in PMC-306 MCs using CRISPR/Cas9, and the effects were studied after TGF-β and/or Ag stimulation. The absence of SMAD2 led to increased proliferation and survival, as well as decreased transcription of target genes like *Smad7* and *Jun* in steady state and after TGF-β treatment. Interestingly, SMAD2 was found to regulate the strength and kinetics of TGF-β-mediated SMAD1/5 activation, resulting in augmented expression of genes like *Id2* and *Id3* in SMAD2-deficient MCs. Unexpectedly, SMAD2 was observed to license Ag-triggered production of pro-inflammatory cytokines, such as IL-6 and TNF, by monitoring expression of secondary repressive signaling elements. Re-introducing SMAD2 restored these events with varying sensitivity depending on the receptor system triggered. Our findings reveal SMAD2 as an initial hub in TGF-β-SMAD1/5 and Ag-FcεRI signaling, offering new possibilities for therapeutic intervention in both TGF-β-controlled and Ag-triggered MC functions using potential SMAD2 activators or inhibitors.

Introduction

Mast cells (MCs) are innate, tissue-resident, granulated hematopoietic cells that develop in characteristic sequential waves from the yolk sac, the fetal liver, and the bone marrow [1]. After birth, immature MCs leave the bone marrow and, following blood passage, enter their target tissues, where they terminally differentiate according to cues of the local environment [1]. In connective tissues, there are long lived connective tissue type MCs and in epithelial tissues at the host-environmental interface there are short lived mucosal, sometimes hypo-granulated MCs [2]. Nevertheless, the highly phenotypic plasticity of MCs achieved due to different environments far exceeds the aforementioned dual categorization [3]. MCs participate in adaptive and innate immune responses and constitute a first line of defense for invading pathogens [4]. To do so, the different MC types are characterized by their individual cargo stored in cytoplasmic vesicles, so-called secretory lysosomes, or by de-novo produced mediators such as arachidonic acid metabolites and cytokines/chemokines [2]. Preformed granular constituents, e.g. histamine and proteases, can be instantaneously released upon stimulation by antigen (Ag) via the high-affinity receptor for IgE (FcεRI). De-novo synthesized mediators are released with delayed kinetics upon the appropriate trigger (e.g. Ag, cytokines, and microbial constituents) [5]. The FcεRI consisting of an IgE-binding α-chain, and ITAM-containing, signaling β- and γ-chains, is central for IgE-mediated allergic activation of MCs [6]. FcεRI activation of MCs leads to the induction of several downstream pathways, including, amongst others, phospholipase C-γ (PLC-γ)-, phosphatidylinositol-3-kinase (PI3K)-, and mitogen-activated protein kinase (MAPK)-controlled pathways, regulating differential pro-inflammatory responses such as degranulation, and lipid mediator as well as cytokine production [5].

TGF-β has been recognized as a key factor to modulate murine and human mucosal MC differentiation and phenotype [7–9]. It was shown that TGF-β regulates responses via non-SMAD

(MAPK) and SMAD pathways which also applies to MCs [10]. Those MAPK responses in MCs include migration and chemotaxis as shown in the human MC line HMC-1 [11]. In addition, TGF-β may govern the switch between proliferation and terminal differentiation of MCs [12]. Moreover, TGF-β has been shown to block proliferation and induce expression of late stage protease effectors [13–15].

Since TGF-β is a pleiotropic ligand involved in a broad array of cellular functions, signaling by this ligand needs to be tightly regulated in space and time [16]. A first regulatory step is the expression of the ligand itself which has been shown to be present in rodent MCs offering the option for autocrine stimulation [17,18]. Importantly, TGF-β is expressed and secreted as a large latent complex that can be proteolytically converted to active TGF-β, for instance by chymase secreted from MCs [17]. Recognition of TGF-β is accomplished by a set of single-span transmembrane receptors, composed of a type I homodimer and a type II homodimer. There are currently seven known type I receptors, which are grouped into bone morphogenetic protein (BMP)-type receptors, ALK1/2/3/6, or TGF-β-type receptors, ALK4/5/7, of which the prototypical TGF-β-receptor is activin receptor-like kinase 5 (ALK5) [19]. However, depending on the mode of signaling, other type I receptors may be involved [20]. After binding of TGF-β to the type II receptor, containing a constitutively active, intracellular Ser/Thr kinase domain, recruitment and transphosphorylation of ALK5 causes activation of its Ser/Thr kinase domain [21]. Interestingly, a subtle receptor tyrosine kinase activity has also been noticed [22]. Thereafter, the type I receptor mediates signal propagation either *via* non-SMAD- or SMAD-dependent pathways [10]. The TGF-β/ALK5 route commonly facilitates activation of the so-called receptor SMADs (R-SMADs) 2 and 3, whereas the BMP/BMP-type I-receptor route leads to activation of the R-SMADs 1/5/9. Alternatively, in several cell types ALK5 in cooperation with BMP-type I receptors also causes activation of SMAD1/5/9 in response to TGF-β [19]. The R-SMADs are composed of an N-terminal MH1-domain, mediating DNA-binding, and a C-terminal MH2-domain, phosphorylated by type I receptors, and thus essential for nuclear transfer and transcriptional activity [23]. MH1 and MH2 domains are connected by a linker domain.

"Regulatory" linker phosphorylation by other kinases, e.g. MAP kinases, can impact nuclear transfer and transcriptional activity of type I receptor activated SMADs [24,25]. However, recent publications also indicate an autonomous function of linker-phosphorylated SMADs [26]. Upon translocation of the activated R-SMADs together with the Co-SMAD SMAD4 into the nucleus, they bind in a context-dependent manner to appropriate promoter elements in complex with cell type specific transcription factors, to regulate target genes in a positive or negative manner [27]. *Smad7* is a prototypically upregulated TGF-β/SMAD2/3 target gene which in turn switches off TGF-β signaling as part of a negative feedback loop [28]. Another group of genes, i.e. *inhibitors of differentiation* (*Id*), are upregulated by TGF-β/SMAD1/5 in epithelial/endothelial cells as well as in MCs in an immediate early manner [12,29,30].

In MCs, most available data focus on TGF-β-regulated gene expression mediated by SMAD2/3, even though TGF-β-mediated SMAD1/5 activation and target gene expression has recently been proven [12]. While *Smad3*-deficient mice (*Smad3*^{delEx8}) are viable [31], *Smad2*-deficient mice are embryonic lethal [32]. Accordingly, the phenotype and biology of SMAD2-deficient (BM)MCs is completely unknown so far.

In this study, we demonstrate extensive crosstalk of TGF-β and Ag signaling, which is manifested on a molecular level by ERK1/2-mediated phosphorylation of the SMAD2 linker region. In addition, using SMAD2-deficient MCs, we proof that TGF-β-induced gene expression functions strictly in a SMAD2-dependent manner, either positively with respect to SMAD2-dependent genes or negatively concerning SMAD1/5-dependent genes. Moreover, the transient activation of SMAD1/5 signaling is sustained in the absence of SMAD2. Finally, we provide evidence that SMAD2 promotes IgE-mediated induction of pro-inflammatory cytokine production, adding to the complexity of the functional cross-talk between regulatory TGF-β and inflammatory Ag-signaling/responses.

Results

SMAD2 integrates TGF-β and FcεRI/ERK signals via differential phosphorylation of its linker and C-terminus

TGF-β signaling relies on phosphorylation of the SMAD2 C-terminus, which can be fine-tuned by signal integration in the SMAD2 linker region, including its phosphorylation upon GPCR-mediated transactivation of the EGF receptor [33]. This indicates that receptors with prominent phospho-tyrosine-based signaling can employ SMAD2 as a signaling module. Therefore, we compared TGF-β- with SCF- as well as Ag-induced engagement of SMAD2 in murine BMMCs. Unlike SCF and Ag, TGF-β stimulation for 5 min caused phosphorylation of the SMAD2 C-terminus, which was slightly enhanced after 15 min (Fig. 1A-C). Further kinetic analysis up to 30 min did not reveal Ag-stimulated SMAD2-CT phosphorylation (Suppl. Fig. 1A-C). On the other hand, 5 min SCF or Ag stimulation led to strong SMAD2-L phosphorylation, while TGF-β only caused a slight response from 15 min on (Fig. 1A-C; Suppl. Fig. 1A-C). A further difference was observed regarding activation of ERK1/2, which were markedly phosphorylated upon SCF and Ag, but not upon TGF-β stimulation (Fig. 1A; Suppl. Fig. 1A). Using the ALK5 inhibitor SB431542, both SMAD2-CT and SMAD2-L phosphorylation in response to TGF-β were clearly shown to be ALK5-dependent (Suppl. Fig. 1D-F).

Since Ag and SCF stimulation resulted in notable SMAD2-L and ERK1/2 phosphorylation (Fig. 1A), we analyzed the pharmacological effect of Trametinib, an inhibitor of the ERK1/2 kinases MEK1/2, on SMAD2-L phosphorylation. Indeed, Ag- and SCF-stimulated P-SMAD2-L was completely inhibited by Trametinib, whereas TGF-β-induced P-SMAD2-CT/P-SMAD2-L were unaffected (Fig. 1D-F).

Recently, we generated a murine peritoneal MC-derived cell line (PMC-306) [34] and applied it to re-analyze the marked differences in TGF-β- vs. Ag-stimulated SMAD2 phosphorylation.

Indeed, as found for BMMCs, TGF-β induced significant SMAD2-CT phosphorylation in PMC-306 MCs, while Ag-stimulated PMC-306 cells showed marked SMAD2-L phosphorylation (Fig. 1G-I). The latter was strongly dependent on the MEK-ERK cascade as shown by the use of Trametinib (Suppl. Fig. 1G-I). Like in BMMCs, TGF-β did not induce ERK phosphorylation in PMC-306 cells (Fig. 1G).

In conclusion, stimulation of MCs (BMMCs and PMC-306) with Ag and SCF results in SMAD2-L phosphorylation dependent on the MEK/ERK MAPK pathway. There is no direct cross-activation beside those ligand effector pairs (TGF/SMAD2-CT *vs.* Ag/SCF/MAPK/ SMAD2-L).

Augmented nuclear P-SMAD2-L translocation upon Ag/TGF-β co-stimulation suppresses TGF-β-induced *Chsy1* expression

SMAD2 acts as a TGF-β-activated transcription factor and its C-terminal phosphorylation plays a central role in nuclear transfer and transcriptional regulation [35]. Next, we aimed at analyzing if Ag impacts the nuclear translocation of SMAD2 on its own and in cross-talk with TGF-β, and its effect on transcription of the TGF-β-responsive genes *Chsy1* (Chondroitin sulfate synthase 1) [36,37] and *Mcpt2* (MC protease 2) [38]. TGF-β caused a shift of P-SMAD2-CT to the nuclear fraction in BMMCs. (Fig. 2A, *left*). In contrast, the nuclear transfer of P-SMAD2-L in the presence of Ag was only allowed if BMMCs were co-stimulated with TGF-β (Fig. 2A, *middle*). Therefore, isolated Ag-driven SMAD2 linker-phosphorylation is not sufficient to mediate SMAD2 nuclear transfer, unless TGF-β/P-SMAD2-CT is active (Fig. 2A).

Next, we analyzed if TGF-β stimulation of BMMCs triggers transcription of *Chsy1* and *Mcpt2* and if this process can be modified by Ag co-stimulation, with the latter treatment causing a shift of dually phosphorylated SMAD2-L/-CT in the nucleus. Indeed, transcription of *Chsy1* and *Mcpt2* was upregulated in response to TGF-β stimulation, which could be suppressed

with Ag co-stimulation, even though these mRNAs were not induced by Ag alone (Fig. 2B/C). We hypothesized that Ag-induced MEK/ERK-mediated SMAD2-L phosphorylation is involved in the observed repression, and that in turn inhibition of MEK might relieve the inhibition of *Chsy1* and *Mcpt2* expression. Trametinib "partially" attenuated the downregulation of *Chsy1* and *Mcpt2* expression in Ag+TGF-β co-stimulated BMMCs (Fig. 2B/C). As expected, Trametinib did not repress TGF-β-stimulated *Chsy1* or *Mcpt2* transcription (Fig. 2B/C).

In order to obtain a more complete picture of the transcriptional landscape of Ag and TGF-β and their cross-talk in BMMCs, cells were treated with or without respective stimuli for 90 min before performing NGS analysis. A heat map of 1777 differentially expressed genes (DEGs; normalized expression across all samples) allowed clear discrimination between non- and TGF-β-stimulated cells vs. Ag- and Ag+TGF-β-stimulated cells, indicating the dominance of Ag-induced signals over TGF-β-induced signals (Fig. 2D; respective volcano blots are shown in Suppl. Fig. 2A). Within these DEGs, 186 genes were found to share the expression pattern of *Chsy1* and *Mcpt2* being upregulated by TGF-β and consecutively downregulated upon TGF-β+Ag co-stimulation (Fig. 2E). Corroborating our results from Fig. 2B/C, *Chsy1* and *Mcpt2* were amongst these genes. On the other hand, transcription of *Smad7*, a gene coding for a negative feedback regulator of TGF-β signaling, was not attenuated upon co-stimulation by TGF-β+Ag vs. TGF-β alone (Fig. 2F/G; Suppl. Fig. 2B). Of note, FcεRI activation alone even resulted in a tendency towards *Smad7* upregulation, which did not always reach statistical significance (Fig. 2F-H; Suppl. Fig. 2B), suggesting that TGF-β-inherent "negative" signaling can be reinforced by FcεRI-mediated activation. In this line, transcription of additional genes coding for negative regulators of i) TGF-β signaling itself (feedback; *Smad7*) or ii) gene transcription (*Strap*, *Tgif1, Skil*, and *Smurf1*) were activated by FcεRI triggering alone (Fig. 2G; Suppl. Fig. 2C). Interestingly, STRAP and SMAD7 have been found to synergize in the inhibition of TGF-β signaling [39].

To further delineate TGF-β-signaling and its modes, we screened our NGS data for differential expression of *Smad* mRNAs. We found that *Smad3*, *Smad6*, and *Smad9* were minimally/not expressed, while *Smad1*, *Smad2*, *Smad4*, *Smad5*, and *Smad7* showed varying but pronounced expression levels (Fig. 2H; Suppl. Fig. 2B). This suggests that BMMCs may engage in TGF-β signaling through SMAD2/4, SMAD1/4, and SMAD5/4 complexes, with negative feedback regulation by SMAD7.

In conclusion, our data suggest that MEK/ERK-mediated SMAD2-L phosphorylation upon Ag stimulation can result in the transcriptional suppression of several TGF-β-induced genes. Conversely, the transcription of another group of genes is enhanced in double-stimulated BMMCs. This implies the presence of complex, situation- and gene-specific regulatory mechanisms in TGF-β + Ag co-stimulated BMMCs.

Deletion of SMAD2 in mast cells modulates identity, vitality and TGF-β-controlled gene expression

We elucidated TGF-β-signaling in MCs in greater depth and focused on the role of SMAD2, since SMAD3 is not expressed in BMMCs and PMC-306 MCs (Fig. 2H; Meurer et al., 2025). We applied CRISPR/Cas9 technology to generate SMAD2-deficient (S2KO) PMC-306 MCs. Three independent S2KO cell lines, along with their respective parental cell lines, were obtained and confirmed through DNA- and RNA-sequencing as well as immunoblotting (Suppl. Fig. 3A-D). Comparing the *Smad2* gRNA sequence with the relevant other receptor SMADs (*Smad1, Smad5*), we expected no side effects (Suppl. Fig. 3E). We started characterizing the different cell lines by comparing the expression of individual receptors. NGS analysis revealed high expression of TGF-β receptors *Tgfbr1 (Alk5), Tgfbr2,* and BMP receptor *Bmpr2* in both parental and S2KO cells (Suppl. Fig. 4). The BMP type I receptors *Acvr1* (*Alk2*) and *Bmpr1a* (*Alk3*) had significantly higher mRNA expression levels in S2KO cells compared to parental cells (Suppl. Fig. 4). In qPCR and Western blot analysis, *Tgfbr1*

(*Alk5*) showed lower expression at both mRNA and protein levels in S2KO cells compared to parental cells. *Tgfbr2* mRNA levels were similar in both parental and S2KO cells, but protein expression appeared to be reduced (Fig. 3A). qPCR of BMP-receptors *Acvr2a*, *Acvr2b*, and *Bmpr2* showed similar expression levels. *Bmpr1a* showed low but upregulated expression in S2KO cells (Fig. 3B). FACS analysis of FcεRI and KIT revealed higher and weaker surface expression, respectively, consistent with mRNA expression levels (*Fcer1a* and *Kit*) analyzed by qPCR, and Western blot for KIT (Fig. 3C), supporting and expanding on data from Zhao et al. in human skin MCs [40].

TGF-β stimulation is known to negatively affect the proliferation and survival of different cell types [41]. Compared to normal peritoneal MCs, PMC-306 cells exhibit accelerated IL-3/SCF-dependent cell cycle progression and show lower cell count/viability in the presence of TGF-β [12,34]. We analyzed if and how TGF-β impacts PMC-306 cell proliferation and viability in the absence of SMAD2. While parental cells showed reduced cell counts and viability with TGF-β treatment for 3 days, these effects were not observed in S2KO cells (Fig. 3D/E). Enhanced proliferation and survival in S2KO cells were accompanied by a significant increase in metabolic activity (Fig. 3F). Additionally, S2KO cells showed diminished phosphorylation of H2A.X, a marker of DNA damage response [42] (Fig. 3G). From our data we excluded the hypothesis that SMAD3 compensates for SMAD2 deficiency, because both parental and S2KO PMC-306 cells showed only very low levels (if at all) of *Smad3* mRNA (see above Fig. 3H; Suppl. Fig. 5A) compared to SMAD3-positive primary hepatic stellate cells (Suppl. Fig. 5B). In principle, mRNA expression of SMAD family members in parental and S2KO PMC-306 cells was qualitatively and quantitatively comparable to BMMCs, with the exception of *Smad1*/SMAD1 (Fig. 3I/J), which showed reduced expression in S2KO cells.

The relevance of SMAD2 for TGF-β-induced transcriptional events was confirmed by analyzing TGF-β target genes in basal conditions. The mRNAs of *Mcpt1 and Jun* as well as JUN protein, were reduced in homeostatic conditions in the absence of SMAD2 (Fig. 3K). In

line, TGF-β-triggered mRNA production of *Jun and Mcpt1* showed no response to TGF-β without SMAD2 (Fig. 4A). In contrast to *Jun and Mcpt1*, *Smad7* and *Skil* still appeared slightly inducible by TGF-β in the absence of SMAD2 (Fig. 4B/C; Suppl. Fig. 5C). As expected, for all mentioned genes a significant dependence on ALK5 could be demonstrated in PMC-306 MCs (Fig. 4A/C) and BMMCs (Fig. 4D) by blocking ALK5 (SB431542) (Fig. 4A/C/D).

In conclusion, PMC-306 cells deficient for SMAD2 already present perturbations in MC biology in homeostatic conditions, with respect to the expression of MC markers, viability and TGF-β target gene expression. Moreover, S2KO PMC-306 cells showed enhanced proliferation and survival compared to parental cells in the presence of TGF-β. Furthermore, our data indicated an exclusive SMAD2 dependence of certain TGF-β target genes (e.g. *Jun*), whereas a different set of TGF-β target genes still showed residual responsiveness in the absence of SMAD2 (e.g. *Skil, Smad7*).

SMAD2-deficiency unleashes SMAD1/5 activity and target gene expression

SMAD-dependent TGF-β-induced cellular activation follows at least two routes, one via SMAD2/3-SMAD4 and another pathway via SMAD1/5-SMAD4 transcriptionally active trimeric complexes [10,19]. Due to the persisting responsiveness of Smad7 and Skil we hypothesized that instead of SMAD2, SMAD1/5 might “still be active” in S2KO PMC-306 MCs. To investigate this, we analyzed our NGS data from TGF-β-stimulated parental and S2KO MCs to identify differentially expressed genes (DEGs), which are still responsive and even upregulated more strongly in S2KO cells. Interestingly, these DEGs included critical targets of TGF-β signaling (e.g. *Id2*, *Id3*) as well as regulators of tyrosine kinases and TLR signaling (e.g. *Spry2*, *Sh2b2*, *Sh2b3*, and *Nfkbia*) (Fig. 5A; Suppl. Fig. 6A). As expected, *Smad7* and *Skil* were strongly dependent on SMAD2 (Fig. 5A). These genes were also upregulated in BMMCs upon TGF-β stimulation (Suppl. Fig. 6B). Expression of *Id* genes is known to be SMAD1/5-dependent and

can be regulated by SMAD3 signaling [12,29,30,43], suggesting reinforcement of SMAD1/5 signaling in SMAD2-deficient MCs. *Id2*/ID2 showed enhanced basal expression in S2KO vs. parental PMC-306 cells (Fig. 5B), and both *Id2* and *Id3* mRNAs were induced stronger in S2KO cells upon TGF-β treatment (Fig. 5C/D). In contrast, *Jun, Mcpt1*, and *Smad7* mRNA levels were significantly higher in TGF-β-stimulated parental cells, indicating for their direct SMAD2-dependence (Fig. 4A/C/D). The increased expression of SMAD1/5-dependent genes in S2KO PMC-306 cells is consistent with enhanced *Acvr1* expression (Suppl. Fig. 4A), as a requirement of two classes of type I receptors, TGFBR1 (ALK5) and ACVR1 (ALK2), for TGF-β-induced phosphorylation of SMAD1/5 has been demonstrated [44]. The involvement of ALK5 in the expression of *Id2* and *Id3* in PMC-306 and BMMC was confirmed by using the ALK5 inhibitor SB431542 (Fig. 5D). Both the effects of TGF-β stimulation and ALK5 inhibition were more pronounced regarding *Id3* compared to *Id2* expression, which is consistent with the increased basal *Id2* expression (Fig. 5C).

Having shown that in the absence of SMAD2 a group of genes are unresponsive and other genes are increased in basal expression and/or upon TGF-β stimulation, we sought to decipher if this regulation takes place at the transcriptional or SMAD activation level. The upregulation of the corresponding receptors *Alk2* and *Alk3* (Suppl. Fig. 4A) led us to analyze SMAD1/5-CT phosphorylation. As depicted in Fig. 5E, parental and S2KO PMC-306 MCs revealed severe kinetic differences in TGF-β-induced P-SMAD1/5-CT. The intensity of P-SMAD1/5-CT was already increased in S2KO cells compared to parental cells after 30 min of TGF-β stimulation, and the respective phosphorylation after 24h showed a more digital pattern. No P-SMAD1/5-CT was detectable in parental cells, whereas signal strength in S2KO PMC-306 cells was not alleviated compared to the 30-min time point. In comparison, P-SMAD2-CT upon TGF-β stimulation of parental cells remained stable over time. Both P-SMAD2-CT and P-SMAD1/5-CT were blocked by the ALK5 inhibitor SB431542 (Fig. 5E). This suggests that SMAD2 limits SMAD1/5 activation via a secondary mechanism, i.e. early

transcription/translation of (a) repressive factor(s), or downregulation of a BMP-receptor (see above).

To interrogate the involvement of type I BMP receptor(s) in TGF-β-induced, SMAD2-controlled transcription of SMAD1/5-dependent genes, we used the ALK2/3 inhibitor LDN193189 (LDN) [45]. Parental and S2KO PMC-306 cells were stimulated with TGF-β or BMP-2 (a strictly SMAD1/5-activating, non-SMAD2-dependent stimulus) for 60 min with/without SB431542 or LDN pretreatment, and phosphorylation of SMAD1/5-CT was analyzed. P-SMAD1/5-CT was markedly stronger in TGF-β vs. BMP-2-stimulated parental cells (Fig. 5F). There was no difference in P-SMAD1/5-CT between both stimuli in S2KO cells (Fig. 5F), suggesting that the presence of SMAD2 generally limits SMAD1/5 activation independent of the stimulus. Indeed, BMP-2 did not induce SMAD2 phosphorylation (Suppl. Fig. 6C). Both inhibitors considerably attenuated TGF-β-stimulated P-SMAD1/5-CT, matching with data by Ramachandran [44]. Intriguingly, inhibition of ALK5 (SB431542) resulted in augmented P-SMAD1/5-CT upon BMP-2 treatment of parental cells, suggesting that basal ALK5 activity decreases BMP-2-mediated activation of SMAD1/5 (Fig. 5F).

qPCR analysis of representative SMAD2-induced (*Jun*) and SMAD2-repressed (*Id2, Id3*) genes confirmed the observed effect of LDN on TGF-β- and BMP-2-induced P-SMAD1/5-CT. LDN pretreatment did not affect the SMAD2 target *Jun* (Suppl. Fig. 6D), but it significantly decreased *Id2* and even more *Id3* expression after TGF-β or BMP2 stimulation (Fig. 5G). The decrease in *Id2* and *Id3* expression by both inhibitors, SB431542 (Fig. 5D) and LDN (Fig. 5G), suggested that TGF-β induces these SMAD1/5 target genes through a complex of ALK5 and ALK2 (or ALK3) [44].

In conclusion, our data support the notion that SMAD2 inhibits SMAD1/5 activation and corresponding transcription in MCs following TGF-β stimulation, likely through a secondary

mechanism. TGF-β stimulation involves a combination of TGFBR1 and possibly ACVR1 to regulate the activation of the SMAD1/5 pathway.

SMAD2 constitutes a signaling hub in mast cell activation downstream of the FcεRI

As shown in Fig. 4C (and Suppl. Fig. 5C), *Smad7* and *Skil* tend to be transcribed upon TGF-β stimulation in a SMAD2-dependent manner. Moreover, Ag stimulation alone was able to cause weak upregulation of *Smad7* and *Skil* (Fig. 2F/G; Fig. 4B; Suppl. Fig. 5C) as well as marked SMAD2-L phosphorylation (Fig. 1). Therefore, we hypothesized that SMAD2 plays a role in the FcεRI-triggered transcription of *Smad7* and *Skil*. Intriguingly, analysis of NGS data from parental and S2KO PMC-306 cells stimulated with Ag for 90 min revealed, among other genes, significantly reduced mRNA expression of *Il6*, *Jun*, and *Nfkbiz* in the absence of SMAD2 (Fig. 6A).

To confirm this finding, we stimulated parental and S2KO PMC-306 cells with Ag for 15 and 90 min and analyzed *Il6* and *Tnf* mRNA expression using RT-qPCR. Whereas there was no difference at the early time point of 15 min (Suppl. Fig. 7A), a dramatic and significant reduction was observed in S2KO cells at the 90 min time point (Fig. 6B). Consistent with the mRNA expression, IL-6 and TNF protein production upon Ag stimulation (t=3h) was almost absent in S2KO cells (Fig. 6C). Since there was minimal difference in *Il6* and *Tnf* mRNA production after 15 min, we reasoned that the signaling defect conveyed by SMAD2-deficiency should appear between 30 and 90 min of Ag stimulation. Indeed, performing kinetic analyses, the reduction of *Il6* and *Tnf* production was increasingly evident starting at approximately 45 min (Fig. 6D; Suppl. Fig. 7B). Since detectable IL-6 and TNF production in parental cells started between 30 and 45 min of Ag stimulation, measurement of these cytokines was hardly possible or difficult in S2KO cells (Fig. 6E; Suppl. Fig. 7C).

Due to these kinetics, we assumed that transcription of these genes (*Il6*, *Tnf*) is dependent on SMAD2 regulating immediate early expression of relevant transcription factors. We hypothesized that SMAD2 deficiency causes either loss of a promoter or gain of a repressor, respectively. Hence, we stimulated BMMCs as well as parental and S2KO PMC-306 cells with Ag in the presence or absence of cycloheximide (CHX) to inhibit translation of immediate early proteins, and measured production of *Tnf* and *Il13* mRNA (Fig.6F/G). Indeed, Ag-induced stimulation of BMMCs and PMC-306 cells in the presence of CHX caused dramatic upregulation ("super-induction") of *Tnf* and *Il13* production, indicating involvement of an immediate-early, suppressively-acting (transcription) factor (Fig. 6F/G). In agreement with SMAD2 repressing (a) suppressive factor(s) upon Ag stimulation, CHX pretreatment restored *Tnf* and *Il13* production in S2KO cells (Fig. 6G).

In conclusion, IgE-mediated activation of pro-inflammatory genes is supported by SMAD2-dependent homeostatic suppression of (an) attenuating (transcription) factor(s). This regulation might allude to attenuation of NFκB signaling in S2KO cells, since several typical NFκB-dependent genes (e.g. *Il1b*, *Nfkbia*, *Nfkb1*, *Tnfaip3*, and *Nlrp3*) were significantly attenuated in Ag-stimulated S2KO cells compared to parental PMC-306 cells (Suppl. Fig. 7D).

Re-expression of SMAD2 differentially restores mast cell effector functions

To directly connect the observed changes with the absence of SMAD2, we re-introduced a V5-tagged version of SMAD2 (V5S2) into the S2KO PMC-306 cells. The finding that S2KO cells proliferated and survived better than parental cells raised the question of whether these cells might be resistant to re-expression of SMAD2. Indeed, repeated attempts to re-express V5S2 in S2KO cells only resulted in reduced SMAD2 protein levels compared to parental cells, even though mRNA expression was significantly increased, as shown by RT-qPCR (Fig. 7A-C; Suppl. Fig. 8A). Despite this, V5S2 appeared to be functional, as TGF-β and Ag

stimulation of these cells led to the expected SMAD2-CT and SMAD2-L phosphorylation, respectively (Fig. 7A/B). Interestingly, upon Ag-stimulation, the induction of *Il6*, *Il13*, and *Tnf* mRNA as well as IL-6 and TNF protein expression were fully restored (Fig. 7D-H), suggesting that the function of SMAD2 in FcεRI signaling does not rely on its full parental expression level.

Hence, we were intrigued to see if the low V5S2 expression is also appropriate to compensate for the SMAD2 deficiency in S2KO cells with respect to TGF-β target genes, and particularly its suppressive effect on SMAD1/5-CT phosphorylation. Analysis of SMAD2-dependent *Jun* and *Smad7* mRNA revealed only partial reversion in the presence of V5S2 (Fig. 7I/J). This finding was confirmed for JUN at the protein level regardless of stimulation time (Fig. 7K/L). However, not all TGF-β-responsive genes were equally (in-) sensitive to the weak SMAD2 reconstitution, as shown by JUN (almost no induction) vs. MCPT1 (strong induction) (Fig. 7L), indicating that protein-type and stability may also mask the effect of weak reconstitution. A decrease in P-SMAD1/5-CT was only observed under basal conditions or after prolonged (24 h) TGF-β stimulation (Fig. 7L). In line, the induction of *Id1*, *Id2* and *Id3* mRNAs was only slightly reduced in V5S2 vs. S2KO PMC-306 cells after TGF-β stimulation (Fig. 7M/N; Suppl. Fig. 8B). This is likely due to the impact of TGF-β on the proliferation and survival of MCs, which only allows for “inadequate” reconstitution of the S2KO cells with V5S2, resulting in correspondingly weak effects with regard to TGF-β stimulation. The complete reversal of the S2KO effects after Ag stimulation is even more surprising, suggesting that the dependence on the number of SMAD2 molecules is much more significant after TGF-β stimulation. Unfortunately, the mechanistic basis for this is not yet known. However, IgE-mediated signaling likely involves more mutually reinforcing elements/pathways that can mask the reduced expression of V5S2.

In conclusion we were able to successfully reconstitute a tagged version of SMAD2 (V5S2) in SMAD2-deficient cells. The introduced SMAD2 was properly phosphorylated upon differential

stimulation, leading to a full reversal of the diminished FcεRI-mediated cytokine expression in S2KO cells. However, it only partially restored TGF-β-mediated target gene expression via SMAD2 (increased expression) or SMAD1/5 (decreased expression). Nonetheless, these experiments support the notion that SMAD2 is directly involved in these regulations and rule out any secondary effect resulting from experimentally induced long-term SMAD2 deficiency.

Discussion

In the current study, we investigated the functional interaction between TGF-β-induced and FcεRI-mediated signaling events in MCs. We specially focused on the pro-inflammatory Ag-triggered functions and their regulation by the TGF-β-activated transcription factor SMAD2, a topic that has not been extensively explored in FcεRI signaling. We demonstrate a significant crosstalk between TGF-β and Ag signaling, with the SMAD2 linker playing a crucial role in integrating both signals. Ablation of SMAD2 underscores its importance in MCs, blunting most "classical" TGF-β responses, and mitigating FcεRI-induced production of pro-inflammatory mediators and regulators. Conversely, a second pathway mediated by SMAD1/5 shifts from transient to sustained kinetics in the absence of SMAD2, demonstrating the regulatory function of SMAD2. In summary, SMAD2 directly influences differentiation and Ag-triggered effector functions in TGF-β- and/or Ag-activated MCs. Additionally, SMAD2 restricts TGF-β signaling pathways by inhibiting SMAD1/5 activation, emphasizing the significance of SMAD2 in MC function.

It is assumed that TGF-β responses are mediated via non-SMAD and SMAD pathways [16]. For the latter, R-SMADs are activated through phosphorylation by the corresponding type I receptor. The ALK5-group and the BMP-group of type I receptors activate the substrates SMAD2/3 and SMAD1/5/9, respectively [19]. SMAD3 and SMAD2 share a very high sequence homology and a common domain structure. However, our studies, using NGS, RT-PCR, and WB, showed no (or only extremely low levels of) expression of *Smad3*/SMAD3 in BMMCs and the PMC-306 MC line. Therefore, we can exclude the possibility that SMAD3 compensates for the loss of SMAD2. To the best of our knowledge, the presence and activation of SMAD3 has been displayed so far only in primary human skin MCs [40]. In order to closely examine TGF-β signaling in MCs, we decided to specifically delete SMAD2, thereby ensuring that we do not "directly" interfere with non-SMAD and SMAD1/5 signaling (as would be the case, when

targeting the receptors). Our thorough analysis coupled with the observation that even in the absence of SMAD2, significant *Smad3* expression was not detectable, suggests that strong SMAD3 expression may not be compatible with MC biology. In the absence of SMAD3, SMAD2 can adopt an anti-proliferative and anti-survival activity, highlighting the differences between SMAD2/3 and SMAD2-only expressing cells.

Using S2KO MCs, we identified a group of genes that were transcribed in a SMAD2-dependent manner upon TGF-β stimulation, such as *Chsy1* and *Smad7*. However, these genes showed two different modes of activation. While *Chsy1* was barely transcribed in response to TGF-β in the absence of SMAD2, *Smad7* appeared responsive even in the absence of SMAD2, albeit at a significantly lower level. This suggests an additional regulatory mechanism beside SMAD2. We were able to demonstrate that this pathway also requires ALK5 and may involve SMAD1/5, which is known to be activated by TGF-β in MCs [12]. Interestingly, different SMAD proteins were found to recognize genome-wide 5-bp GC motifs [52], potentially enabling the induction of transcription of the same genes by both SMAD2 and SMAD1. Since TGF-β-stimulated *Mcpt1* and *Mcpt2* transcription in BMMCs was reported to be dependent on both SMAD2/4 and GATA1/2 [15], differential co-regulation of promoters by a combination of transcription factors and epigenetic regulators might explain why some genes are activated by SMAD2 or SMAD1 only, while others are activated by both. Although SMAD1/5 are more commonly known for their activation during BMP stimulation, their activation by the TGF-β/ALK1 axis in endothelial cells has been demonstrated [53,54]. However, ALK1 (ACVRL1) was not detectable in the MCs studied. Ramachandran et al. demonstrated that TGF-β-mediated SMAD1/5 activation is also facilitated by the two type-I receptors ALK5 and ACVR1 (also known as ALK2) [44]. Consistent with this, it was shown that *Smad7* can be transcribed in a SMAD1- and GATA-dependent manner [55]. Meanwhile, several modes of TGF-β-mediated SMAD1/5 activation have been published, relying on different BMP type-I receptors or on ALK5 alone [35,56,57]. It is important to note that the expression of the corresponding BMP-type-I receptors is relatively low in MCs, as well as their sensitivity

towards BMPs. In turn, ALK3 expression along with responsiveness to BMP-2 increases in the absence of SMAD2, suggesting a functional availability of ALK3 in S2KO MCs.

We have recently shown that in contrast to the prolonged TGF-β-mediated SMAD2 activation, phosphorylation of SMAD1/5 and the corresponding target gene expression is only transient [12]. Activation of SMAD1/5 could be extended in the presence of the translation inhibitor CHX, implying a secondary response in the timed deactivation of SMAD1/5. In the present study, we demonstrate that this deactivation of SMAD1/5 is due to the presence of SMAD2, as ablation of SMAD2 extends the activation/phosphorylation of SMAD1/5 and their target gene *Id2*. The mechanism involved may include a combination of transcription and dephosphorylation and/or ubiquitination-dependent degradation [58]. Several Ser/Thr-phosphatases have been found to be capable of dephosphorylating SMAD1-CT, such as PPM1A [59], CTDSP1, CTDSP2 [60], and PDP1 [61]. Knocking down CTDSPs via siRNA not only increased the level, but also the duration of SMAD1 phosphorylation. Although all these phosphatases were expressed at the mRNA level, no significant differences were noted between parental and S2KO PMC-306 cells. NEDD4L, a central E3 ubiquitin ligase in the TGF-β signaling pathway, is equally expressed in parental and S2KO MCs, and does not seem to be relevant for SMAD1 degradation [62]. Interestingly, *Acvr1* (*Alk2*) expression was significantly stronger in S2KO cells, which, considering the data from Ramachandran et al. [44], may result in prevalent TGF-β-induced SMAD1-CT phosphorylation. It is possible that a different kinase is able to phosphorylate SMAD1 in the absence of SMAD2. In conclusion, we find that SMAD2, through its control of gene expression, can act as a negative regulator of SMAD1/5. However, since cell type- and/or situation-dependent co-factors may be necessary for TGF-β/SMAD2-regulated SMAD1/5 activity, this conundrum cannot be definitely answered at this time.

The situation in S2KO MCs under study (enhanced and prolonged TGF-β-induced C-terminal SMAD1/5 phosphorylation, and TGF-β-triggered, SMAD1/5-dependent expression of *Id2*/ID2)

should be a promising cellular system to identify additional SMAD1/5-dependent genes and mechanisms. Based on the NGS analysis of TGF-β-stimulated S2KO and parental MCs, at least four further negative feedback regulators, in addition to SMAD7 and SKIL, might be transcribed dependent on SMAD1/5, in a SMAD2-deficient or in a particularly SMAD1/5-activated situation: *Spry2*, *Nfkbia*, *Sh2b2*, and *Sh2b3*. NFKBIA (IκBα) is known as the dominant feedback inhibitor of the classical NFκB pathway [63], SPRY2 (SPROUTY2) acts as a negative feedback regulator of receptor tyrosine kinase signaling [64]. SH2B2 (also known as APS), a PH- and SH2-domain containing adapter protein, can inhibit JAK-STAT signaling [65]. Likewise, another ubiquitous member of the SH2B family, SH2B3 (also known as LNK), is functioning, amongst others, as negative regulator in the course of growth factor receptor signaling [66]. Hence, SMAD1/5 signaling in a cell type- and situation-dependent manner, might constitute a so far unrecognized signaling module with respect to TGF-β-mediated control of NFκB and (receptor) tyrosine kinase signaling.

On a cellular basis, TGF-β has been reported as a negative regulator of MC proliferation and survival, and a promoter of MC differentiation [8]. Additionally, studies have shown that MCs play a role in TGF-β-driven pathophysiological settings such as fibrogenic processes [67,68]. Our data support the concept that SMAD2 can serve as an integration hub between signaling processes initiated by different receptors. Since TGF-β is both a crucial MC differentiation factor and an anti-inflammatory mediator, SMAD2-mediated integration can guide MCs towards specific decisions based on their surrounding micro-environment. Our recent study [12], along with current data, confirm that TGF-β can alter cellular responses such as proliferation (induced by the IL-3 receptor) and production of pro-inflammatory cytokines (triggered by FcεRI activation). Intriguingly, simultaneous stimulation with Ag and TGF-β can have bidirectional effects: TGF-β can influence Ag-induced transcription of cytokines like *Il6*, *Il13*, and *Tnf.* Conversely, Ag co-stimulation can impact TGF-β-induced transcription of genes typically responsive to TGF-β, such as *Id3, Chsy1, Mcpt1,* and *Mcpt2*. Given that TGF-β

controls the differentiation of MCs, particularly mucosal MCs [8,9], crosslinking of FcεRI may alter the differentiation pathway and enable a phenotypical switch in MCs depending on the specific situation.

It has been emphasized previously that Ag stimulation affects the TGF-β1/SMAD2-mediated transcriptional response. Receptor-mediated phosphorylation of the C-terminal MH2 residues is a crucial step for nuclear transfer and transcriptional activity [35]. However, the presence of Ag signaling did not impact TGF-β-mediated C-terminal phosphorylation of SMAD2. Along with ALK5-mediated Ser phosphorylation of the MH2 C-terminal domain, a cluster of three Ser residues in the SMAD2 linker region can be phosphorylated by different MAP kinases [26]. EGF-induced Ser phosphorylation of the SMAD2 linker region inhibited SMAD2´s nuclear translocation [69], while ERK1-mediated linker phosphorylation enhanced SMAD2 stability, leading to increased transcription [70]. Therefore, linker phosphorylation of SMAD2 can have either a negative or positive effect on downstream TGF-β signaling. In vascular smooth muscle cells, it has been observed that various ligands, such as LPS and TGF-β, induce *Chsy1* through SMAD2 serine linker phosphorylation [71,72]. Although TGF-β and Ag may share MAPKs in other cell types, we could show that activation of p38, JNK and ERK1/2 is specifically triggered by Ag in MCs. Consequently, we could show here in MCs for the first time that there is a prominent phosphorylation of the SMAD2 linker region upon Ag stimulation, which was dependent on MEK/ERK activation. However, this linker-phosphorylated SMAD2 does not translocate into the nucleus without additional TGF-β-mediated C-terminal phosphorylation, arguing against a respective autonomous linker function [26]. A further consequence of linker phosphorylation might be the generation of docking sites for interacting proteins. In MCs, there are no data so far analyzing SMAD2-linker phosphorylation and its consequences for signaling and gene regulation. Only one paper identified an interaction of MITF with the linker region of SMAD(2)/3, but this interaction appeared to have no functional consequence [73].

Another unexpected finding from our study was the promotion of IgE-mediated cytokine production by SMAD2, which limits the expression of negative regulator(s). Ag-triggered "super-induction" of *Tnf* and *Il13* in presence of CHX suggests limitation of *Tnf* transcription by a SMAD2-dependent suppressive transcription factor. Moreover, several typical NFκB-controlled mRNAs (such as *IL1b*, *Nfkbia*, *Nlrp3*, and *Tnfaip3*) were significantly attenuated upon Ag stimulation in S2KO vs. parental MCs. Intriguingly, *Nr4a2* mRNA was upregulated more strongly in Ag-triggered SMAD2-deficient cells (Fig. 6A). NR4A2 (also known as NURR1) has been shown to repress NFκB function in microglia and astrocytes [74], as well as limit the inflammatory profile of pro-inflammatory macrophages [75]. However, when the pharmacological NR4A2 activator IP7e was applied [75], attenuation of Ag-induced *Tnf* production was not achieved. This suggests that an additional SMAD2-controlled factor restrains pro-inflammatory gene expression in MCs.

Final conclusions

SMAD2 constitutes a multifunctional signaling hub in TGF-β- and Ag- stimulated MCs. Based on our finding of IgE-mediated, MEK/ERK-dependent SMAD2-L phosphorylation we decided to generate and analyze SMAD2-deficient MCs. This allowed us to decipher the role of SMAD2 in inter-SMAD pathway regulation and the homeostatic control of Ag-triggered cytokine production. NGS and bioinformatics analyses revealed a mutually repressive signaling constellation with SMAD2 as an important element in both TGF-β- and Ag-dependent MC activation. The development of pharmacological SMAD2 inhibitors would offer the possibility of targeted strengthening of SMAD1/5 function, thereby enhancing the attenuating function of TGF-β.

Data limitations and perspectives

The commercially available polyclonal anti-P-SMAD2-L antibody lacks selectivity for individual phosphorylation sites within the linker region. However, complete suppression of Ag-induced SMAD2-L phosphorylation by the MEK inhibitor Trametinib implicates involvement of the MEK/ERK pathway while excluding contributions from other kinases. The mechanistic interplay between FcεRI-mediated events and TGF-β-induced signaling remains incompletely resolved, particularly regarding spatiotemporal regulation, kinases involved, and epigenetic modulatory events. Nuclear cooperation or repression of differentially activated transcription factors or cytosolic phosphorylation events and resulting protein interactions could play a role. Of interest in this respect are the dual-specificity phosphorylation capabilities of TGFBR2 and TGFBR1, which could bridge Ser-/Thr-phosphorylation-based TGF-β receptor and Tyr-phosphorylation-guided FcεRI signaling [22,76]. Our identification of SMAD2-mediated repression of SMAD1/5 raises a critical question: Could cytosolic SMAD2 inhibition during TGF-β stimulation enhance SMAD1/5 activation (e.g. by pharmacological means)? According to our present data on negative feedback regulators, this might result in augmented suppressive function of TGF-β. Our unexpected data on FcεRI-induced pro-inflammatory functions of SMAD2 leaves some key questions unresolved. Does SMAD2 act in the nuclear or the cytosolic compartment of MCs to control IgE-mediated inflammatory responses? Moreover, since Ag triggers immediate-early *Tgfb*/TGF-β transcription/translation, what are the roles of MC proteases (e.g., chymase and granzyme B) in autocrine, latent TGF-β conversion?

Material and Methods

Key resources tables

Antibodies	Source	Identifier	Dilution
Goat Anti-Histon H4 (C-20)	Santa Cruz	sc-8658	1:1000
Goat Anti-KIT (M-14)	Santa Cruz	sc-1494	1:500
Hamster Anti-FcεRIα (MAR-1) FITC	eBioscience	11-5898-85	1:100
Mouse Anti-GAPDH (6C5)	Santa Cruz	sc-32233	1:1000
Mouse Anti-Histon H4 (L64C1)	Cell Signaling	#2935	1:1000
Mouse Anti-SMAD2 (L16D3)	Cell Signaling	#3103	1:1000
Mouse Anti-V5 (SV5-Pk1)	Invitrogen	R960-25	1:2500
Mouse Anti-β-Actin (AC-15)	Sigma-Aldrich	A5441	1:10000
Rabbit Anti-ERK1/2	Cell Signaling	#9102	1:1000
Rabbit Anti-HSP90 (C45G5)	Cell Signaling	#4877	1:1000
Rabbit Anti-ID2 (C-20)	Santa Cruz	sc-489	1:500
Rabbit Anti-JUN	Cell Signaling	#9165	1:1000
Rabbit Anti-KIT (C-19)	Santa Cruz	sc-168	1:500
Rabbit Anti-P-ERK1/2 (Thr202/Tyr204) (D13.14.4E)	Cell Signaling	#4370	1:1000
Rabbit Anti-P-H2A.X (Ser139) (20E3)	Cell Signaling	#9718	1:1000
Rabbit Anti-P-SMAD1(Ser463/465)/ P-SMAD5 (Ser463/465)/P-SMAD9 (Ser465/467) (D5B10)	Cell Signaling	#13820	1:1000
Rabbit Anti-P-SMAD2 (Ser245/250/255)	Cell Signaling	#3104	1:1000
Rabbit Anti-P-SMAD2 (Ser465/467)/ P-SMAD3 (Ser423/425) (D27F4)	Cell Signaling	#8828	1:1000
Rabbit Anti-SMAD1	Cell Signaling	#9743	1:1000
Rabbit Anti-TβRI (ALK5) (V-22)	Santa Cruz	sc-398	1:500
Rabbit Anti-TβRII (L-21)	Santa Cruz	sc-400	1:500
Rat Anti-CD117 (ACK45) PE	BD Pharmingen	553869	1:100
Rat Anti-MCPT1	R&D Systems	MAB5146	1:500

Chemicals, peptides and recombinant proteins	Source	Identifier
BMP-2	R&D Systems	#355-BM
Cycloheximide	Sigma-Aldrich	#239763-M
DNP-HSA	Sigma-Aldrich	A6661
LDN193189 dihydrochloride	Biotechne/TOCRIS	#6053
SB431542	Sigma-Aldrich	S4317
SCF	PeproTech	#250-03
TGF-β1	R&D Systems	#7666-MB-005

Trametinib	Selleckchem	S2673

RT-qPCR Primer	Primer sequence (5′ ⟶ 3′)	
Gene	Forward	Reverse
Actb	CTCTAGACTTCGAGCAGGAGATGG	ATGCCACAGGATTCCATACCCAAGA
Acvr2a	AAGATGCCCTACCCTCCTGT	TTGAGCAACTGGGCTTTCCA
Acvr2b	CTTCTCTGGGGATCCCTGTG	CTCCCAGTTGGCGTTGTAGT
Bmpr1a	TCTTCTCCAGCTGCTTTTGCT	ATCACGGTTGTAACGACCCC
Bmpr2	GAGCACAGAGGCCCAATTCT	GCCATCTTGTGTTGACTCACCT
Chsy1	AGAAATACCTGCAGACCCGC	GGCACCACTGGAATGGGTAT
Fcer1a	GTGTACTTGAATGTAACGCAAGA	GGACTAAGACCATGTCAGCAGAT
Gapdh	ACTCAAGATTGTCAGCAATGCA	TGGTCATGAGCCCTTCCACAA
Id1	GCGAGATCAGTGCCTTGG	CTCCTGAAGGGCTGGAGTC
Id2	GACAGAACCAGGCGTCCA	AGCTCAGAAGGGAATTCAGATG
Id3	TCCGCATCTCCCGATCCA	TTCCCATGCAAGCCTCCCT
Il13	GGCAGCATGGTATGGAGTGT	CTTGCGGTTACAGAGGCCAT
Il6	TCCAGTTGCCTTCTTGGGAC	GTGTAATTAAGCCTCCGACTTG
Jun	ACATGCTCAGGGAACAGGTG	CTGCGTTAGCATGAGTTGGC
Kit	GATCTGCTCTGCGTCCTGTT	CTTGCAGATGGCTGAGACG
Mcpt1	ACGGACAGAGGTTCTGAGGA	GAGCTCCAAGGGTGACAGTG
Mcpt2	TTCACCACTAAGAACGGTTCG	CTCCAAGGATGACACTGATTTCA
Nr4a2	Qiagen QuantiTect Primer Assay (QT00106407)	
Smad1	CTACTGGCGCAGTCTGTGAA	GATCTCAATCCAGCAGGGGG
Smad2	AGGACGGTTAGATGAGCTTGAG	GTCCCCAAATTTCAGAGCAA
Smad2 + Smad2ΔExon3	AGGACGGTTAGATGAGCTTGAG	CCTGAAGACGGCCATCAAG
Smad3	CGCAGGTTCTCCAAACCTCT	AATGTCTCCCCAACTCGCTG
Smad5	AATAAAGTTGCGGCGCGTG	CTTGACAGGTGCCATAGGCT
Smad7	ACCCCCATCACCTTAGTCG	GAAAATCCATTGGGTATCTGGA
Tgfbr1	GCAGCTCCTCATCGTGTTG	AGAGGTGGCAGAAACACTGTAAT
Tgfbr2	AGAAGCCGCATGAAGTCTG	GGCAAACCGTCTCCAGAGTA
Tnf	AGCACAGAAAGCATGATCCGC	TGCCACAAGCAGGAATGAGAAG

Experimental model

Animals and cell culture:

All mice used in this study were either on a C57BL/6 background or on a mixed C57BL/6 x 129/Sv background. Experiments were conducted in compliance with German legislation

governing animal studies and following the principles of laboratory animal care. The mice were housed at the Institute of Laboratory Animal Science, Medical Faculty of RWTH Aachen University, which holds a license for the husbandry and breeding of laboratory animals from the veterinary office of the Städteregion Aachen (administrative district). The institute adheres to a quality management system that is certified according to DIN EN ISO 9001:2015. All protocols are reviewed by a Governmental Animal Care and Use Committee at the Landesamt für Natur-, Umwelt- und Verbraucherschutz, Recklinghausen (LANUV). No human samples were used, and no experiments were conducted involving living animals. Mice were sacrificed by cervical dislocation to isolate cells from femurs in order to obtain bone marrow cells, which were differentiated into BMMCs as previously described [77].

BMMCs were cultivated as single-cell suspensions in growth medium (RPMI 1640, Gibco Thermo Fisher, #21875-091) containing 15 % heat-inactivated FCS (Capricorn, #FBS-12A or PAN, #P30-3306), 100 units/ml Penicillin and 100 µg/ml Streptomycin (Sigma, #P0781), 10 mM HEPES (Sigma, #H0887), 100 µM β-mercaptoethanol (Sigma, #M6250), and 30 ng/mL IL-3 from X63-Ag8-653 conditioned medium [78]. PMC-306 were cultivated in similar growth medium conditions containing 10% heat-inactivated FCS and with the addition of 5 ng/mL SCF derived from cell culture supernatant from CHO cells that were transfected with an expression vector coding for murine SCF [77]. The differentiation of BMMCs was evaluated after 4-5 weeks in culture by FACS analysis (see below) and considered successful if more than 95% of BMMCs were positive for MC surface markers FcεRI and KIT. For analysis of BMMCs via Western blot and RT-qPCR (see below), cells were starved (RPMI 1640 + 10% FCS without IL-3) overnight, while BMMCs were not starved for the other experiments. PMC-306 cells were not starved. Additionally, cells were pre-loaded with 0.15 µg/ml IgE (clone SPE-7, Sigma-Aldrich, #D8406) overnight when stimulated with DNP-HSA on the following day.

CRISPR-Cas9-mediated KO in PMC-306

PMC-306 cells were used to establish a Smad2 KO cell line. A single-guide RNA (sgRNA) complex was created by combining 200 µM crisprRNA against Smad2 (IDT, predesigned Alt-R CRISPR-Cas9 gRNA, sequence: TTCACCACTGGCGGAGTGAA) and 200 µM ATTO550 labeled tracrRNA (IDT, #1075927) at 95 °C for 5 min, followed by cooling to room temperature. Subsequently, 120 pM sgRNA and 104 pM Cas9 enzyme (IDT, #1081058) were mixed in duplex buffer (IDT, #11-01-03-01) and incubated for 15 min at room temperature. 2 x 10^6 PMC-306 cells along with 1 µl electroporation enhancer (IDT, #1075915) were added and cells were electroporated using the Neon Transfection system (Thermo Fisher, #MPK10096) at 1600 V for 30 mS with one pulse. The cells were then transferred to pre-warmed medium without Penicillin and Streptomycin. The next day, ATTO550 positive cells were individually sorted into 96-well plates by the Flow Cytometry Facility at the Uniklinik Aachen using the BD FACS Aria Fusion cell sorter. Single cells were expanded and subsequently analyzed via Western blot (see below). Smad2 KO clones were sequenced and analyzed with the CRISPR analysis tool by Synthego [79]. Three clones with homozygous mutations on both alleles were selected for experiments.

Retroviral transduction in PMC-306

PMC-306 Smad2 parental and KO cells were used to re-introduce Smad2. Platinum-E cells (Cell Biolabs, #RV-101) were transfected with a construct containing 3xV5-Smad2 and puromycin using the TransIT-LT1 Transfection Reagent (Mirus, #22073360) according to the manufacturer's instruction and incubated for 24 h. The medium was changed, and the cells were then incubated for an additional 24 h. The retrovirus-containing supernatant was collected, sterile filtered and mixed with the Retro-X Concentrator (Takara, #631455) following the manufacturer's instructions. The mixture was incubated for at least 6 h at 4 °C and then centrifuged at 1500 x g for 45 min at 4 °C. The pellet was resuspended in PMC-306 growth medium and combined with PMC-306 cells along with 8 µg/ml Polybrene (Merck, #TR-1003-G). On the following day, harvesting of the retrovirus-containing supernatant was repeated, added to the PMC-306 cells and incubated for another 24 h. PMC-306 were centrifuged and

resuspended in medium containing 8 μg/ml puromycin (InvivoGen, #ant-pr) for selection. After successful selection, single clones were generated using a dilution series. These clones were propagated and analyzed by Western blot (see below).

Next generation sequencing

3'mRNA sequencing libraries were prepared using the Lexogen QuantSeq 3'mRNA-Seq v2 Library Prep Kit FWD with Unique Dual Indexes (UDIs) following the manufacturer's protocol. Prior to library preparation, the concentration of RNA was measured using the Promega Quantus Fluorometer. Additionally, the size distribution of the RNA was assessed using the Agilent TapeStation with an RNA ScreenTape. Quantification and quality assessment were repeated after library preparation, again using the Quantus fluorometer and the Agilent TapeStation with a High Sensitivity D1000 ScreenTape. Libraries were denatured, diluted, and loaded onto a NextSeq High Output v2.5 (75 cycles) flow cell. A 1% PhiX control library was spiked in to improve base calling accuracy. Single-end sequencing was performed with 75 cycles on the Illumina NextSeq platform according to the manufacturer's instructions.

FASTQ files were generated using bcl2fastq (Illumina). To ensure reproducible analysis, samples were processed using the publicly available nf-core/RNA-seq pipeline version 3.12 [80] implemented in Nextflow 23.10.0 [81] with minimal command. In brief, lane-level reads were trimmed using Trim Galore 0.6.7 [82] and aligned to the mouse genome (GRCm39) using STAR 2.7.9a [83]. Gene-level and transcript-level quantification was performed using Salmon v1.10.1 [84]. All analysis was conducted using custom scripts in R version 4.3.2 with the DESeq2 v.1.32.0 framework [85].

ELISA

For the analysis of IL-6 and TNF secretion, MCs were pre-loaded overnight with IgE and ELISA plates (Corning, #9018) were coated with capturing anti-IL-6 (1:250, BD Biosciences, #554400) or anti-TNF (1:250, R&D Systems, #AF-410-NA) antibodies diluted in PBS at 4 °C

overnight. Cells were resuspended in stimulation medium (RPMI 1640, #32404 + 0.1 % BSA, Serva, #11930) and the cell number was adjusted to 1.2 x 10^6 cells/ml. After the cells adapted to 37 °C, they were stimulated for the indicated time points and the supernatant was collected. ELISA plates were washed three times with PBS + 0.1% Tween and blocked with PBS + 2% BSA for 2 h (for IL-6 ELISA) or PBS + 1% BSA + 5 % sucrose for 90 min (for TNF-α ELISA) at room temperature. The plates were washed again and loaded with the cell supernatant (50 µl for IL-6 and 100 µl for TNF-α) as well as a standard dilution for IL-6 (BD Pharmingen, #554582) and TNF (R&D Systems, #410-MT-010). ELISA plates were incubated overnight at 4 °C. Afterwards, the ELISA plates were washed three times and incubated with biotinylated anti-IL-6 (1:500, BD Biosciences, #554402) or anti-TNF (1:250, R&D Systems, #BAF410) antibodies diluted in PBS + 1% BSA for 45 min (for IL-6 ELISA) or 2 h (for TNF-α ELISA) at room temperature. The plates were washed again and incubated with streptavidin alkaline phosphatase (1:1000, BD Pharmingen, #554065) diluted in PBS + 0.5 % BSA for 30 min (for IL-6 ELISA) or 45 min (for TNF-α ELISA) at room temperature. The plates were washed three times and the substrate p-nitro-phenyl-phosphate (Sigma-Aldrich, #S0942, 1 tablet dissolved in 5 ml 2 mM $MgCl_2$ in 50 mM sodium carbonate) was added. A plate reader (BioTek Eon) was used to measure OD at 450 nm.

Flow cytometry

Flow cytometry was used to analyze the surface marker expression of MCs. To confirm the successful differentiation of BMMCs, cells were washed in FACS buffer (PBS + 3 % FCS + 0.1 % sodium azide) and incubated with FITC-coupled anti-FcεRI (1:100, clone MAR-1, eBioscience, #11-5898-85) and PE-coupled anti-CD117 (KIT, 1:100, clone ACK45, BD Pharmingen, #553869) for 30 min at 4 °C in the dark. After another wash, the cells were analyzed using flow cytometry using a FACS Canto II flow cytometer (BD Biosciences). The acquired flow cytometry data were then analyzed using FlowJo software v10.

Proliferation, Viability and XTT assays

PMC-306 parental and KO cells were seeded at a density of 0.2 x 10^6 cells/mL and treated as indicated. After 24 hours of incubation in a humidified atmosphere (at 37°C with 5% CO_2), the cells were resuspended and 50 µl of the cell suspension was diluted in 10 ml of PBS. Cell count and viability were determined using a Casy cell counter from Innovatis. The cell count was monitored over a period of 72 hours.

Metabolic activity was assessed using the XTT cell proliferation kit II (Roche, #11465015001). PMC-306 Smad2 parental and KO cells were plated at a density of 0.3 x 10^6 cells/ml a 96-well microplate with a final volume of 100 µl. After 72 hours of incubation under humidified culture conditions (37 °C, 5% CO_2), metabolic activity was measured by adding XTT reagent to each well following the manufacturer's instructions. Absorbance was then read at 492 nm with a reference wavelength of 650 nm using a plate reader. Total absorbance was calculated by subtracting the absorbance at 650 nm from the absorbance at 492 nm.

Western blot

Cells were adjusted to a concentration of 1-5 x 10^6 cells/mL in stimulation medium and stimulated as indicated in the respective experiments. Stimulation was halted by snap-freezing in liquid nitrogen. Pellets were lysed in phosphorylation solubilization buffer containing 50 mM HEPES, 100 mM sodium fluoride, 10 mM sodium pyrophosphate, 2 mM EDTA, 2 mM sodium molybdate, 2 mM sodium orthovanadate, 0.5 % NP-40, 0.3 % sodium deoxycholate, 0.03 % sodium dodecylsulfate, 1 µM PMSF (Sigma, #P7626), 10 µg/mL Aprotinin (Applichem, #A2132), 2 µg/mL Leupeptin (Roth, CN33.1) for 30 min at 4 °C. Lysates were centrifuged for 10 min at 16000 x g and 4 °C, the supernatant was supplemented with loading buffer (30 mM Tris, 2 % glycerol, 2.5 % β-mercaptoethanol, 1% SDS, 0.02% bromophenol blue) and samples were heated at 95 °C for 5 min. Samples were separated on 10 – 15 % SDS polyacrylamide gels using SDS running buffer (25 mM Tris, 192 mM glycine, 0.1 % SDS). Proteins were electroblotted onto PVDF membrane (Roth, #T830.1) and unspecific binding sites were blocked in 5 % non-fat milk powder in PBST (137 mM NaCl, 2.7 mM KCl, 10 mM Na_2HPO_4,

2,5 mM KH_2PO_4, 0.1 % Tween 20, pH 6.9) for 1h. Most primary antibodies were diluted in 1 % BSA in PBST, while anti-SMAD2 and anti-P-SMAD2 antibodies were diluted in 5% BSA in TBST (20 mM Tris, 150 mM NaCl, 0.05% Tween 20 , pH 7.2). Detection was done using horseradish-peroxidase-conjugated secondary antibodies (Dako, #P0448, #P0160, #P0161) and Clarity Max Western ECL Substrate (Biorad, #1705062). Proteins were visualized using a LAS-4000 reader (Fujifilm).

Western blots shown in Figs. 1A, 1D, 1G, 2A, 7A, 7B and Suppl. Fig. 1A, 1D, 1G, 3D, 8A were carried out according to the protocol described above, while Western blots in Figs. 3A, 3C, 3G, 3J, 3K, 5B, 5E, 5F, 7K, 7L and Suppl. Fig. 6C were performed as described previously[12].

qPCR

Total RNA was isolated from 3-5 x 10^6 cells using the NucleoSpin RNA Plus Kit (Macherey Nagel, #740984) according to the manufacturer's instructions. 1 µg of RNA was reverse transcribed using random oligonucleotides (Roche, #11034731.001) and the Omniscript Reverse Transcription Kit (Qiagen, #205113) according to the manufacturer's instructions. Quantification of transcript expression was carried out using the SensiMix SYBR No-Rox Kit (Bioline, QT650-05) and 10 pmol of specific primers. PCR reactions were conducted on a Rotorgene Q (Qiagen). Transcript expression was normalized to the housekeeping genes *Gapdh* or *Actb* and relative expression was calculated using the delta-C_T method [86].

qPCRs shown in Figs. 2B, 2C, 2F, 6B, 6D, 6F, 6G, 7D, 7E, 7F and Suppl. Figs. 7A, 7B were carried out according to the protocol described above, while qPCRs in Figs. 3A, 3B, 3C, 3I, 3K, 4A, 4C, 4D, 5B, 5D, 5G, 7C, 7I, 7J, 7M, 7N and Suppl. Figs. 5C, 6D, 8B were performed as described previously[12].

Statistical analysis

All data shown were generated from at least three independent experiments. Statistical analysis and graphing of data were performed using Prism (v10.4.1, GraphPad, SanDiego, USA). All statistical test procedures were done as described in the respective figure legends.

p-values were considered statistically significant according to the style in GraphPad Prism (ns: $p>0.05$, * $p<0.05$, ** $p<0.01$, *** $p<0.001$, **** $p<0.0001$). The respective number of independent biological replicates per experiment is indicated in the figure legends.

Data availability atatement

The NGS data have been deposited in NCBI´sGene Expression Omnibus and are accessible through the GEO Series accession numbers GSE?????? And GSE??????. (These accession numbers will be disclosed upon final submission)

Acknowledgements

This work was supported by grants from the Deutsche Forschungsgemeinschaft (DFG) (HU794/14-1 to MH, LI1045/6-1 to CL, WE2554/15-1 to RW and ME3431/2-1 to SM).

References

1. St John, A.L., Rathore, A.P.S., and Ginhoux, F. (2023). New perspectives on the origins and heterogeneity of mast cells. Nat Rev Immunol *23*, 55–68. https://doi.org/10.1038/s41577-022-00731-2.

2. Valent, P., Akin, C., Hartmann, K., Nilsson, G., Reiter, A., Hermine, O., Sotlar, K., Sperr, W.R., Escribano, L., George, T.I., et al. (2020). Mast cells as a unique hematopoietic lineage and cell system: From Paul Ehrlich's visions to precision medicine concepts. Theranostics *10*, 10743–10768. https://doi.org/10.7150/thno.46719.

3. Dwyer, D.F., Barrett, N.A., Austen, K.F., and Immunological Genome Project, C. (2016). Expression profiling of constitutive mast cells reveals a unique identity within the immune system. Nat Immunol *17*, 878–887. https://doi.org/10.1038/ni.3445.

4. Galli, S.J., Gaudenzio, N., and Tsai, M. (2020). Mast Cells in Inflammation and Disease: Recent Progress and Ongoing Concerns. Annu Rev Immunol *38*, 49–77. https://doi.org/10.1146/annurev-immunol-071719-094903.

5. Huber, M., Cato, A.C.B., Ainooson, G.K., Freichel, M., Tsvilovskyy, V., Jessberger, R., Riedlinger, E., Sommerhoff, C.P., and Bischoff, S.C. (2019). Regulation of the pleiotropic effects of tissue-resident mast cells. J Allergy Clin Immunol *144*, S31–S45. https://doi.org/10.1016/j.jaci.2019.02.004.

6. Huber, M. (2013). Activation/Inhibition of mast cells by supra-optimal antigen concentrations. Cell Commun Signal *11*, 7. https://doi.org/10.1186/1478-811X-11-7.

7. Haque, T.T., and Frischmeyer-Guerrerio, P.A. (2022). The Role of TGFbeta and Other Cytokines in Regulating Mast Cell Functions in Allergic Inflammation. Int. J. Mol. Sci. *23*. https://doi.org/10.3390/ijms231810864.

8. Derakhshan, T., Samuchiwal, S.K., Hallen, N., Bankova, L.G., Boyce, J.A., Barrett, N.A., Austen, K.F., and Dwyer, D.F. (2021). Lineage-specific regulation of inducible and constitutive mast cells in allergic airway inflammation. J Exp Med *218*. https://doi.org/10.1084/jem.20200321.

9. Derakhshan, T., Hollers, E., Perniss, A., Ryan, T., McGill, A., Hacker, J., Bergmark, R.W., Bhattacharyya, N., Lee, S.E., Maxfield, A.Z., et al. (2025). Human intraepithelial mast cell differentiation and effector function are directed by TGF-beta signaling. J Clin Invest *135*. https://doi.org/10.1172/JCI174981.

10. Aashaq, S., Batool, A., Mir, S.A., Beigh, M.A., Andrabi, K.I., and Shah, Z.A. (2022). TGF-beta signaling: A recap of SMAD-independent and SMAD-dependent pathways. J Cell Physiol *237*, 59–85. https://doi.org/10.1002/jcp.30529.

11. Olsson, N., Piek, E., Sundstrom, M., ten Dijke, P., and Nilsson, G. (2001). Transforming growth factor-beta-mediated mast cell migration depends on mitogen-activated protein kinase activity. Cell Signal *13*, 483–490. https://doi.org/10.1016/s0898-6568(01)00176-0.

12. Meurer, S.K., Bronneberg, G., Penners, C., Kauffmann, M., Braunschweig, T., Liedtke, C., Huber, M., and Weiskirchen, R. (2025). TGF-beta1 Induces Mucosal Mast Cell Genes and is Negatively Regulated by the IL-3/ERK1/2 Axis. Cell Commun Signal *23*, 76. https://doi.org/10.1186/s12964-025-02048-8.

13. Funaba, M., Ikeda, T., Murakami, M., Ogawa, K., and Abe, M. (2005). Up-regulation of mouse mast cell protease-6 gene by transforming growth factor-beta and activin in mast cell progenitors. Cell Signal *17*, 121–128. https://doi.org/10.1016/j.cellsig.2004.06.005.

14. Funaba, M., Ikeda, T., Murakami, M., Ogawa, K., Nishino, Y., Tsuchida, K., Sugino, H., and Abe, M. (2006). Transcriptional regulation of mouse mast cell protease-7 by TGF-beta. Biochim Biophys Acta *1759*, 166–170. https://doi.org/10.1016/j.bbaexp.2006.04.003.

15. Kasakura, K., Nagata, K., Miura, R., Iida, M., Nakaya, H., Okada, H., Arai, T., Arai, T., Kawakami, Y., Kawakami, T., et al. (2020). Cooperative Regulation of the Mucosal Mast Cell-Specific Protease Genes Mcpt1 and Mcpt2 by GATA and Smad Transcription Factors. J Immunol *204*, 1641–1649. https://doi.org/10.4049/jimmunol.1900094.

16. Massague, J., and Sheppard, D. (2023). TGF-beta signaling in health and disease. Cell *186*, 4007–4037. https://doi.org/10.1016/j.cell.2023.07.036.

17. Lindstedt, K.A., Wang, Y., Shiota, N., Saarinen, J., Hyytiainen, M., Kokkonen, J.O., Keski-Oja, J., and Kovanen, P.T. (2001). Activation of paracrine TGF-beta1 signaling upon stimulation and degranulation of rat serosal mast cells: a novel function for chymase. FASEB J *15*, 1377–1388. https://doi.org/10.1096/fj.00-0273com.

18. Funaba, M., Nakaya, K., Ikeda, T., Murakami, M., Tsuchida, K., and Sugino, H. (2006). Requirement of Smad3 for mast cell growth. Cell Immunol *240*, 47–52. https://doi.org/10.1016/j.cellimm.2006.06.002.

19. Heldin, C.H., and Moustakas, A. (2016). Signaling Receptors for TGF-beta Family Members. Cold Spring Harb Perspect Biol *8*. https://doi.org/10.1101/cshperspect.a022053.

20. Derynck, R., and Budi, E.H. (2019). Specificity, versatility, and control of TGF-beta family signaling. Sci Signal *12*. https://doi.org/10.1126/scisignal.aav5183.

21. Huang, F., and Chen, Y.G. (2012). Regulation of TGF-beta receptor activity. Cell Biosci *2*, 9. https://doi.org/10.1186/2045-3701-2-9.

22. Lee, M.K., Pardoux, C., Hall, M.C., Lee, P.S., Warburton, D., Qing, J., Smith, S.M., and Derynck, R. (2007). TGF-beta activates Erk MAP kinase signalling through direct phosphorylation of ShcA. EMBO J *26*, 3957–3967. https://doi.org/10.1038/sj.emboj.7601818.

23. Macias, M.J., Martin-Malpartida, P., and Massague, J. (2015). Structural determinants of Smad function in TGF-beta signaling. Trends Biochem Sci *40*, 296–308. https://doi.org/10.1016/j.tibs.2015.03.012.

24. Kretzschmar, M., Doody, J., and Massague, J. (1997). Opposing BMP and EGF signalling pathways converge on the TGF-beta family mediator Smad1. Nature *389*, 618–622. https://doi.org/10.1038/39348.

25. Liang, J., Zhou, Y., Zhang, N., Wang, D., Cheng, X., Li, K., Huang, R., Lu, Y., Wang, H., Han, D., et al. (2021). The phosphorylation of the Smad2/3 linker region by nemo-like kinase regulates TGF-beta signaling. J Biol Chem *296*, 100512. https://doi.org/10.1016/j.jbc.2021.100512.

26. Kamato, D., and Little, P.J. (2020). Smad2 linker region phosphorylation is an autonomous cell signalling pathway: Implications for multiple disease pathologies. Biomed Pharmacother *124*, 109854. https://doi.org/10.1016/j.biopha.2020.109854.

27. Hill, C.S. (2016). Transcriptional Control by the SMADs. Cold Spring Harb Perspect Biol *8*. https://doi.org/10.1101/cshperspect.a022079.

28. Nakao, A., Afrakhte, M., Moren, A., Nakayama, T., Christian, J.L., Heuchel, R., Itoh, S., Kawabata, M., Heldin, N.E., Heldin, C.H., et al. (1997). Identification of Smad7, a TGFbeta-inducible antagonist of TGF-beta signalling. Nature *389*, 631–635. https://doi.org/10.1038/39369.

29. Kang, Y., Chen, C.R., and Massague, J. (2003). A self-enabling TGFbeta response coupled to stress signaling: Smad engages stress response factor ATF3 for Id1 repression in epithelial cells. Mol Cell *11*, 915–926. https://doi.org/10.1016/s1097-2765(03)00109-6.

30. Lebrin, F., Goumans, M.J., Jonker, L., Carvalho, R.L., Valdimarsdottir, G., Thorikay, M., Mummery, C., Arthur, H.M., and ten Dijke, P. (2004). Endoglin promotes endothelial cell proliferation and TGF-beta/ALK1 signal transduction. EMBO J *23*, 4018–4028. https://doi.org/10.1038/sj.emboj.7600386.

31. Yang, X., Letterio, J.J., Lechleider, R.J., Chen, L., Hayman, R., Gu, H., Roberts, A.B., and Deng, C. (1999). Targeted disruption of SMAD3 results in impaired mucosal immunity and diminished T cell responsiveness to TGF-beta. EMBO J *18*, 1280–1291. https://doi.org/10.1093/emboj/18.5.1280.

32. Nomura, M., and Li, E. (1998). Smad2 role in mesoderm formation, left-right patterning and craniofacial development. Nature *393*, 786–790. https://doi.org/10.1038/31693.

33. Dayati, P., Rezaei, H.B., Sharifat, N., Kamato, D., and Little, P.J. (2018). G protein coupled receptors can transduce signals through carboxy terminal and linker region phosphorylation of Smad transcription factors. Life Sci *199*, 10–15. https://doi.org/10.1016/j.lfs.2018.03.004.

34. Capellmann, S., Sonntag, R., Schuler, H., Meurer, S.K., Gan, L., Kauffmann, M., Horn, K., Konigs-Werner, H., Weiskirchen, R., Liedtke, C., et al. (2023). Transformation of primary murine peritoneal mast cells by constitutive KIT activation is accompanied by loss of Cdkn2a/Arf expression. Front Immunol *14*, 1154416. https://doi.org/10.3389/fimmu.2023.1154416.

35. Wrighton, K.H., Lin, X., and Feng, X.H. (2009). Phospho-control of TGF-beta superfamily signaling. Cell Res *19*, 8–20. https://doi.org/10.1038/cr.2008.327.

36. Rostam, M.A., Shajimoon, A., Kamato, D., Mitra, P., Piva, T.J., Getachew, R., Cao, Y., Zheng, W., Osman, N., and Little, P.J. (2018). Flavopiridol Inhibits TGF-beta-Stimulated Biglycan Synthesis by Blocking Linker Region Phosphorylation and Nuclear Translocation of Smad2. J Pharmacol Exp Ther *365*, 156–164. https://doi.org/10.1124/jpet.117.244483.

37. Kamato, D., Burch, M., Zhou, Y., Mohamed, R., Stow, J.L., Osman, N., Zheng, W., and Little, P.J. (2019). Individual Smad2 linker region phosphorylation sites determine the expression of proteoglycan and glycosaminoglycan synthesizing genes. Cell Signal *53*, 365–373. https://doi.org/10.1016/j.cellsig.2018.11.005.

38. Pemberton, A.D., Brown, J.K., Wright, S.H., Knight, P.A., and Miller, H.R. (2006). The proteome of mouse mucosal mast cell homologues: the role of transforming growth factor beta1. Proteomics *6*, 623–631. https://doi.org/10.1002/pmic.200500211.

39. Datta, P.K., and Moses, H.L. (2000). STRAP and Smad7 synergize in the inhibition of transforming growth factor beta signaling. Mol Cell Biol *20*, 3157–3167. https://doi.org/10.1128/MCB.20.9.3157-3167.2000.

40. Zhao, W., Gomez, G., Yu, S.H., Ryan, J.J., and Schwartz, L.B. (2008). TGF-beta1 attenuates mediator release and de novo Kit expression by human skin mast cells through a Smad-dependent pathway. J Immunol *181*, 7263–7272. https://doi.org/10.4049/jimmunol.181.10.7263.

41. Deng, Z., Fan, T., Xiao, C., Tian, H., Zheng, Y., Li, C., and He, J. (2024). TGF-beta signaling in health, disease, and therapeutics. Signal Transduct Target Ther *9*, 61. https://doi.org/10.1038/s41392-024-01764-w.

42. Yuan, J., Adamski, R., and Chen, J. (2010). Focus on histone variant H2AX: to be or not to be. FEBS Lett *584*, 3717–3724. https://doi.org/10.1016/j.febslet.2010.05.021.

43. Yang, J., Davies, R.J., Southwood, M., Long, L., Yang, X., Sobolewski, A., Upton, P.D., Trembath, R.C., and Morrell, N.W. (2008). Mutations in bone morphogenetic protein type II receptor cause dysregulation of Id gene expression in pulmonary artery smooth muscle cells: implications for familial pulmonary arterial hypertension. Circ Res *102*, 1212–1221. https://doi.org/10.1161/CIRCRESAHA.108.173567.

44. Ramachandran, A., Vizan, P., Das, D., Chakravarty, P., Vogt, J., Rogers, K.W., Muller, P., Hinck, A.P., Sapkota, G.P., and Hill, C.S. (2018). TGF-beta uses a novel mode of receptor activation to phosphorylate SMAD1/5 and induce epithelial-to-mesenchymal transition. Elife *7*. https://doi.org/10.7554/eLife.31756.

45. Yu, P.B., Deng, D.Y., Lai, C.S., Hong, C.C., Cuny, G.D., Bouxsein, M.L., Hong, D.W., McManus, P.M., Katagiri, T., Sachidanandan, C., et al. (2008). BMP type I receptor inhibition reduces heterotopic [corrected] ossification. Nat Med *14*, 1363–1369. https://doi.org/10.1038/nm.1888.

46. Labbe, E., Silvestri, C., Hoodless, P.A., Wrana, J.L., and Attisano, L. (1998). Smad2 and Smad3 positively and negatively regulate TGF beta-dependent transcription through the forkhead DNA-binding protein FAST2. Mol Cell *2*, 109–120. https://doi.org/10.1016/s1097-2765(00)80119-7.

47. Dennler, S., Huet, S., and Gauthier, J.M. (1999). A short amino-acid sequence in MH1 domain is responsible for functional differences between Smad2 and Smad3. Oncogene *18*, 1643–1648. https://doi.org/10.1038/sj.onc.1202729.

48. Shi, Y., Wang, Y.F., Jayaraman, L., Yang, H., Massague, J., and Pavletich, N.P. (1998). Crystal structure of a Smad MH1 domain bound to DNA: insights on DNA binding in

TGF-beta signaling. Cell *94*, 585–594. https://doi.org/10.1016/s0092-8674(00)81600-1.

49. Zhou, S., Zawel, L., Lengauer, C., Kinzler, K.W., and Vogelstein, B. (1998). Characterization of human FAST-1, a TGF beta and activin signal transducer. Mol Cell *2*, 121–127. https://doi.org/10.1016/s1097-2765(00)80120-3.

50. Kashyap, M., Bailey, D.P., Gomez, G., Rivera, J., Huff, T.F., and Ryan, J.J. (2005). TGF-beta1 inhibits late-stage mast cell maturation. Exp Hematol *33*, 1281–1291. https://doi.org/10.1016/j.exphem.2005.07.001.

51. Kanamaru, Y., Sumiyoshi, K., Ushio, H., Ogawa, H., Okumura, K., and Nakao, A. (2005). Smad3 deficiency in mast cells provides efficient host protection against acute septic peritonitis. J Immunol *174*, 4193–4197. https://doi.org/10.4049/jimmunol.174.7.4193.

52. Martin-Malpartida, P., Batet, M., Kaczmarska, Z., Freier, R., Gomes, T., Aragon, E., Zou, Y., Wang, Q., Xi, Q., Ruiz, L., et al. (2017). Structural basis for genome wide recognition of 5-bp GC motifs by SMAD transcription factors. Nat Commun *8*, 2070. https://doi.org/10.1038/s41467-017-02054-6.

53. Goumans, M.J., Valdimarsdottir, G., Itoh, S., Lebrin, F., Larsson, J., Mummery, C., Karlsson, S., and ten Dijke, P. (2003). Activin receptor-like kinase (ALK)1 is an antagonistic mediator of lateral TGFbeta/ALK5 signaling. Mol Cell *12*, 817–828. https://doi.org/10.1016/s1097-2765(03)00386-1.

54. Sanchez-Duffhues, G., Williams, E., Goumans, M.J., Heldin, C.H., and Ten Dijke, P. (2020). Bone morphogenetic protein receptors: Structure, function and targeting by selective small molecule kinase inhibitors. Bone *138*, 115472. https://doi.org/10.1016/j.bone.2020.115472.

55. Benchabane, H., and Wrana, J.L. (2003). GATA- and Smad1-dependent enhancers in the Smad7 gene differentially interpret bone morphogenetic protein concentrations. Mol Cell Biol *23*, 6646–6661. https://doi.org/10.1128/MCB.23.18.6646-6661.2003.

56. Daly, A.C., Randall, R.A., and Hill, C.S. (2008). Transforming growth factor beta-induced Smad1/5 phosphorylation in epithelial cells is mediated by novel receptor complexes and is essential for anchorage-independent growth. Mol Cell Biol *28*, 6889–6902. https://doi.org/10.1128/MCB.01192-08.

57. Liu, I.M., Schilling, S.H., Knouse, K.A., Choy, L., Derynck, R., and Wang, X.F. (2009). TGFbeta-stimulated Smad1/5 phosphorylation requires the ALK5 L45 loop and mediates the pro-migratory TGFbeta switch. EMBO J *28*, 88–98. https://doi.org/10.1038/emboj.2008.266.

58. Schmierer, B., Tournier, A.L., Bates, P.A., and Hill, C.S. (2008). Mathematical modeling identifies Smad nucleocytoplasmic shuttling as a dynamic signal-interpreting system. Proc Natl Acad Sci U S A *105*, 6608–6613. https://doi.org/10.1073/pnas.0710134105.

59. Duan, X., Liang, Y.Y., Feng, X.H., and Lin, X. (2006). Protein serine/threonine phosphatase PPM1A dephosphorylates Smad1 in the bone morphogenetic protein signaling pathway. J Biol Chem *281*, 36526–36532. https://doi.org/10.1074/jbc.M605169200.

60. Knockaert, M., Sapkota, G., Alarcon, C., Massague, J., and Brivanlou, A.H. (2006). Unique players in the BMP pathway: small C-terminal domain phosphatases dephosphorylate Smad1 to attenuate BMP signaling. Proc Natl Acad Sci U S A *103*, 11940–11945. https://doi.org/10.1073/pnas.0605133103.

61. Chen, H.B., Shen, J., Ip, Y.T., and Xu, L. (2006). Identification of phosphatases for Smad in the BMP/DPP pathway. Genes Dev *20*, 648–653. https://doi.org/10.1101/gad.1384706.

62. Gao, S., Alarcon, C., Sapkota, G., Rahman, S., Chen, P.Y., Goerner, N., Macias, M.J., Erdjument-Bromage, H., Tempst, P., and Massague, J. (2009). Ubiquitin ligase Nedd4L targets activated Smad2/3 to limit TGF-beta signaling. Mol Cell *36*, 457–468. https://doi.org/10.1016/j.molcel.2009.09.043.

63. Ferreiro, D.U., and Komives, E.A. (2010). Molecular mechanisms of system control of NF-kappaB signaling by IkappaBalpha. Biochemistry *49*, 1560–1567. https://doi.org/10.1021/bi901948j.

64. Puranik, N., Jung, H., and Song, M. (2024). SPROUTY2, a Negative Feedback Regulator of Receptor Tyrosine Kinase Signaling, Associated with Neurodevelopmental Disorders: Current Knowledge and Future Perspectives. Int J Mol Sci *25*. https://doi.org/10.3390/ijms252011043.

65. Wakioka, T., Sasaki, A., Mitsui, K., Yokouchi, M., Inoue, A., Komiya, S., and Yoshimura, A. (1999). APS, an adaptor protein containing Pleckstrin homology (PH) and Src homology-2 (SH2) domains inhibits the JAK-STAT pathway in collaboration with c-Cbl. Leukemia *13*, 760–767. https://doi.org/10.1038/sj.leu.2401397.

66. Devalliere, J., and Charreau, B. (2011). The adaptor Lnk (SH2B3): an emerging regulator in vascular cells and a link between immune and inflammatory signaling. Biochem Pharmacol *82*, 1391–1402. https://doi.org/10.1016/j.bcp.2011.06.023.

67. Bradding, P., and Pejler, G. (2018). The controversial role of mast cells in fibrosis. Immunol Rev *282*, 198–231. https://doi.org/10.1111/imr.12626.

68. Weiskirchen, R., Meurer, S.K., Liedtke, C., and Huber, M. (2019). Mast Cells in Liver Fibrogenesis. Cells *8*. https://doi.org/10.3390/cells8111429.

69. Kretzschmar, M., Doody, J., Timokhina, I., and Massague, J. (1999). A mechanism of repression of TGFbeta/ Smad signaling by oncogenic Ras. Genes Dev *13*, 804–816. https://doi.org/10.1101/gad.13.7.804.

70. Funaba, M., Zimmerman, C.M., and Mathews, L.S. (2002). Modulation of Smad2-mediated signaling by extracellular signal-regulated kinase. J Biol Chem *277*, 41361–41368. https://doi.org/10.1074/jbc.M204597200.

71. Afroz, R., Zhou, Y., Little, P.J., Xu, S., Mohamed, R., Stow, J., and Kamato, D. (2020). Toll-like Receptor 4 Stimulates Gene Expression via Smad2 Linker Region Phosphorylation in Vascular Smooth Muscle Cells. ACS Pharmacol Transl Sci *3*, 524–534. https://doi.org/10.1021/acsptsci.9b00113.

72. Rostam, M.A., Kamato, D., Piva, T.J., Zheng, W., Little, P.J., and Osman, N. (2016). The role of specific Smad linker region phosphorylation in TGF-beta mediated expression of glycosaminoglycan synthesizing enzymes in vascular smooth muscle. Cell Signal *28*, 956–966. https://doi.org/10.1016/j.cellsig.2016.05.002.

73. Funaba, M., Ikeda, T., Murakami, M., Ogawa, K., Tsuchida, K., Sugino, H., and Abe, M. (2003). Transcriptional activation of mouse mast cell Protease-7 by activin and transforming growth factor-beta is inhibited by microphthalmia-associated transcription factor. J Biol Chem *278*, 52032–52041. https://doi.org/10.1074/jbc.M306991200.

74. Saijo, K., Winner, B., Carson, C.T., Collier, J.G., Boyer, L., Rosenfeld, M.G., Gage, F.H., and Glass, C.K. (2009). A Nurr1/CoREST pathway in microglia and astrocytes protects

dopaminergic neurons from inflammation-induced death. Cell *137*, 47–59. https://doi.org/10.1016/j.cell.2009.01.038.

75. Solis-Barbosa, M.A., Santana, E., Munoz-Torres, J.R., Segovia-Gamboa, N.C., Patino-Martinez, E., Meraz-Rios, M.A., Samaniego, R., Sanchez-Mateos, P., and Sanchez-Torres, C. (2024). The nuclear receptor Nurr1 is preferentially expressed in human pro-inflammatory macrophages and limits their inflammatory profile. Int Immunol *36*, 111–128. https://doi.org/10.1093/intimm/dxad048.

76. Lawler, S., Feng, X.H., Chen, R.H., Maruoka, E.M., Turck, C.W., Griswold-Prenner, I., and Derynck, R. (1997). The type II transforming growth factor-beta receptor autophosphorylates not only on serine and threonine but also on tyrosine residues. J Biol Chem *272*, 14850–14859. https://doi.org/10.1074/jbc.272.23.14850.

77. Meurer, S.K., Ness, M., Weiskirchen, S., Kim, P., Tag, C.G., Kauffmann, M., Huber, M., and Weiskirchen, R. (2016). Isolation of Mature (Peritoneum-Derived) Mast Cells and Immature (Bone Marrow-Derived) Mast Cell Precursors from Mice. PLoS One *11*, e0158104. https://doi.org/10.1371/journal.pone.0158104.

78. Karasuyama, H., and Melchers, F. (1988). Establishment of mouse cell lines which constitutively secrete large quantities of interleukin 2, 3, 4 or 5, using modified cDNA expression vectors. Eur J Immunol *18*, 97–104. https://doi.org/10.1002/eji.1830180115.

79. Conant, D., Hsiau, T., Rossi, N., Oki, J., Maures, T., Waite, K., Yang, J., Joshi, S., Kelso, R., Holden, K., et al. (2022). Inference of CRISPR Edits from Sanger Trace Data. CRISPR J *5*, 123–130. https://doi.org/10.1089/crispr.2021.0113.

80. Ewels, P.A., Peltzer, A., Fillinger, S., Patel, H., Alneberg, J., Wilm, A., Garcia, M.U., Di Tommaso, P., and Nahnsen, S. (2020). The nf-core framework for community-curated

bioinformatics pipelines. Nat Biotechnol *38*, 276–278. https://doi.org/10.1038/s41587-020-0439-x.

81. Di Tommaso, P., Chatzou, M., Floden, E.W., Barja, P.P., Palumbo, E., and Notredame, C. (2017). Nextflow enables reproducible computational workflows. Nat Biotechnol *35*, 316–319. https://doi.org/10.1038/nbt.3820.

82. Krueger, F., James, F., Ewels, P., Afyounian, E., and Schuster, B. (2021). FelixKrueger/TrimGalore: v0.6.7 - DOI via Zenodo. Preprint at Zenodo, https://doi.org/https://doi.org/10.5281/zenodo.5127899 https://doi.org/https://doi.org/10.5281/zenodo.5127899.

83. Dobin, A., Davis, C.A., Schlesinger, F., Drenkow, J., Zaleski, C., Jha, S., Batut, P., Chaisson, M., and Gingeras, T.R. (2013). STAR: ultrafast universal RNA-seq aligner. Bioinformatics *29*, 15–21. https://doi.org/10.1093/bioinformatics/bts635.

84. Patro, R., Duggal, G., Love, M.I., Irizarry, R.A., and Kingsford, C. (2017). Salmon provides fast and bias-aware quantification of transcript expression. Nat Methods *14*, 417–419. https://doi.org/10.1038/nmeth.4197.

85. Love, M.I., Huber, W., and Anders, S. (2014). Moderated estimation of fold change and dispersion for RNA-seq data with DESeq2. Genome Biol *15*, 550. https://doi.org/10.1186/s13059-014-0550-8.

86. Pfaffl, M.W. (2001). A new mathematical model for relative quantification in real-time RT-PCR. Nucleic Acids Res *29*, e45. https://doi.org/10.1093/nar/29.9.e45.

Figure Legends

Figure 1. SMAD2-L phosphorylation upon FcεRI crosslinking is dependent on MEK/ERK activation

(A-C) Representative Western blots for P-SMAD2-CT (S465/467), P-SMAD2-L (S245/250/255), and P-ERK1/2 (T202/Y204) of protein extracts from BMMCs in response to 5 and 15 min of TGF-β (1 ng/mL), 5 min of SCF (30 ng/mL), and 5 min of Ag (20 ng/mL). HCl was used as a control for TGF stimulation. HSP90 served as the loading control. Asterisks indicate detection on the same membrane. (B and C) Quantitative analysis of P-SMAD2-CT and P-SMAD2-L protein levels relative to HSP90 from three independent experiments are shown as mean + SD. *p<0.05, **p<0.01 by one-way ANOVA and Tukey's multiple comparison test.

(D-F) Representative Western blots for P-SMAD2-CT, P-SMAD2-L, and P-ERK1/2 of protein extracts from BMMCs in response to 15 min of TGF-β (1 ng/mL), 5 min Ag (20 ng/mL), and 5 min of SCF (30 ng/mL) with pre-incubation of 30 min of Trametinib (50 nM) or DMSO control. HSP90 served as the loading control. Asterisks indicate detection on the same membrane. Non-relevant lanes were removed from the blot. The removal is indicated by a dashed line. (E and F) Quantitative analysis of P-SMAD2-CT and P-SMAD2-L protein levels relative to HSP90 from three independent experiments are shown as mean + SD. *p<0.05, **p<0.01, ***p<0.001, ****p<0.0001 by two-way ANOVA and Tukey's multiple comparison test.

(G-I) Representative Western blots for P-SMAD2-CT, P-SMAD2-L, Smad2, and P-ERK1/2, of protein extracts from PMC-306 cells in response to 15 min of TGF-β (1 ng/mL), 15 min of Ag (20 ng/mL), and 15 min of SCF (30 ng/mL). HCl was used as a control for TGF stimulation. HSP90 served as loading control. Asterisks indicate detection on the same membrane. (H and I) Quantitative analysis of P-SMAD2-CT and P-SMAD2-L protein levels relative to HSP90 from three independent experiments are shown as mean + SD. *p<0.05, **p<0.01, ***p<0.001, ****p<0.0001 by one-way ANOVA and Tukey's multiple comparison test.

Figure 2. Situation- and gene-dependent mutual regulation of TGF-β and Ag co-stimulation.

(A) Representative cytosol-nucleus-fractionation for P-SMAD2-CT (S465/467), P-SMAD2-L (S245/250/255) and SMAD2 of protein extracts from BMMCs in response to 30 min of Ag (20 ng/mL), TGF-β (1 ng/mL) and Ag + TGF-β. GAPDH served as loading control for the cytosolic fraction, while Histon H4 served as the loading control for the nuclear fraction.

(B and C) The mRNA expression of *Chsy1* (B) and *Mcpt2* (C) were assessed by RT-qPCR in BMMCs in response to 90 min of Ag (20 ng/mL), TGF-β (1 ng/mL) and Ag + TGF-β with pre-incubation of 30 min of Trametinib (50 nM) or DMSO control. The mRNA expression was normalized to *Gapdh*. Three independent experiments are shown as mean + SD. *p<0.05, **p<0.01 by two-way ANOVA and Tukey's multiple comparison test.

(D) Heatmap of genes differentially expressed from BMMCs in response to 90 min of TGF-β (1 ng/mL), Ag (2 ng/mL) and Ag + TGF-β. Rows represent genes and columns represent samples of three independent experiments. The color scale indicates the normalized read counts in log10 scale.

(E) The Venn diagram illustrates the overlap of differentially expressed genes between two experimental conditions. Each circle represents a set of genes significantly altered. The upper circle represents 1540 genes downregulated after Ag + TGF-β stimulation compared to TGF-β treatment, while the lower circle represents 284 genes upregulated after TGF-β stimulation compared to control. The central overlap shows genes regulated across both conditions.

(F) The mRNA expression of *Smad7* was assessed by RT-qPCR in BMMCs in response to 90 min of Ag (20 ng/mL), TGF-β (1 ng/mL) and Ag + TGF-β. The mRNA expression was normalized to *Actb*. Three independent experiments are shown as mean + SD. *p<0.05 by one-way ANOVA and Tukey's multiple comparison test.

(G) Heatmap of genes differentially expressed from BMMCs in response to 90 min of Ag (2 ng/mL) and Ag + TGF-β (1 ng/mL). Rows represent genes and columns represent samples of three independent experiments. The color scale indicates the normalized read counts in log10 scale.

(H) Heatmap of genes differentially expressed from BMMCs in response to 90 min of Ag (2 ng/mL) + TGF-β (1 ng/mL). Rows represent genes and columns represent samples of three independent experiments. The color scale indicates the normalized read counts in log10 scale.

Figure 3. Basic evaluation of SMAD2-deficient (S2KO) MCs.

(A) The mRNA expression of *Tgfbr1* and *Tgfbr2* was assessed by RT-qPCR in resting PMC-306 parental and S2KO cells. The mRNA expression was normalized to *Actb*. Each replicate is represented by a different symbol. Three independent experiments are shown as mean + SD. *p<0.05, **p<0.01 by unpaired *t*-test. Expression of ALK5 and TβRII in protein extracts from resting PMC-306 cells was analyzed by Western Blot, with β-Actin serving as a loading control.

(B) The mRNA expression of *Bmpr1a, Bmpr2, Acvr2a* and *Acvr2b* was assessed by RT-qPCR in resting PMC-306 parental and S2KO cells. The mRNA expression was normalized to *Actb*. Each replicate is represented by a different symbol. Three independent experiments are shown as mean + SD. *p<0.05, **p<0.01 by unpaired *t*-test.

(C) Flow cytometric analysis of the cell surface expression of FcεR1α and KIT in resting PMC-306 parental and S2KO cells. Data from three independent experiments are depicted as mean fluorescence intensity (MFI) + SD. The mRNA expression of *Fcer1a* and *Kit* was assessed by RT-qPCR in resting PMC-306 parental and S2KO cells. The mRNA expression was normalized to *Actb*. Each replicate is represented by a different symbol. Three independent experiments are shown as mean + SD. *p<0.05, **p<0.01 by unpaired t-test. Expression of KIT in protein extracts from resting PMC-306 parental and S2KO cells was analyzed by Western blot, with ERK1/2 serving as the loading control.

(D and E) Cell count (D) and viability (E) of PMC-306 parental and S2KO cells in the presence or absence of TGF-β (1 ng/mL) were measured every 24 h for up to 72 using a CASY cell counter. Data from three independent experiments are shown as mean + SD. *p<0.05, **p<0.01 by two-way ANOVA and Tukey's multiple comparison test.

(F) The metabolic activity of PMC-306 parental and S2KO cells after 72 h of cultivation was determined by XTT assay. Each replicate is represented by a different symbol. Data from three independent experiments are shown as mean + SD. *p<0.05 by unpaired t-test.

(G) Western blot analysis for SMAD2 and P-H2A.X (S139) in protein extracts from resting PMC-306 parental and S2KO cells. HSP90 and β-Actin served as loading control.

(H) Heatmap of *Smad* genes differentially expressed in resting PMC-306 parental and S2KO cells. Rows represent genes and columns represent samples from three independent experiments. The color scale indicates the normalized read counts in log10 scale.

(I) The mRNA expression of *Smad1, Smad2, and Smad5* was assessed by RT-qPCR in resting PMC-306 parental and S2 KO cells. The mRNA expression was normalized to *Actb*. Each replicate is represented by a different symbol. Three independent experiments are shown as mean + SD. *p<0.05 by unpaired t-test.

(J) Western blot analysis for SMAD1 and SMAD2 in protein extracts from resting PMC-306 parental and S2KO cells. ERK1/2 and β-Actin served as loading controls. Asterisks indicate detection on the same membrane.

(K) The mRNA expression of *Mcpt1* and *Jun* was assessed by RT-qPCR in resting PMC-306 parental and S2KO cells. The mRNA expression was normalized to *Actb*. Each replicate is represented by a different symbol. Three independent experiments are shown as mean + SD. *p<0.05 by unpaired t-test. Expression of JUN in protein extracts from resting PMC-306 S2parental and S2KO cells was analyzed by Western blot, with GAPDH serving as a loading control.

Figure 4. Verification of SMAD2-dependent transcriptional events using S2KO MCs.

(A) The mRNA expression of *Jun* and *Mcpt1* was assessed by RT-qPCR in PMC-306 parental and S2KO cells in response to 90 min of TGF-β (1 ng/mL) with pre-incubation of 60 min of SB431542 (5 μM) or DMSO control. The mRNA expression was normalized to *Actb*. Each replicate is represented by a different symbol. Three independent experiments are shown as

mean + SD. *p<0.05, **p<0.01, ***p<0.001, ****p<0.0001 by two-way ANOVA and Tukey's multiple comparison test.

(B) Differentially expressed *Smad7* gene from PMC-306 parental and S2KO cells in response to 90 min of Ag (2 ng/mL), TGF-β (1 ng/mL), and Ag+TGF-β. Floating bars display the normalized read counts (NGS analysis). Each replicate is represented by a dot. *p<0.05, **p<0.01, ***p<0.001, ****p<0.0001 by two-way ANOVA and Tukey's multiple comparison test.

(C) The mRNA expression of *Smad7* was assessed by RT-qPCR in PMC-306 parental and S2KO cells in response to 90 min of TGF-β (1 ng/mL) with pre-incubation of 60 min of SB431542 (5 μM) or DMSO control. The mRNA expression was normalized to *Actb*. Each replicate is represented by a different symbol. Three independent experiments are shown as mean + SD. *p<0.05, **p<0.01, ***p<0.001, ****p<0.0001 by two-way ANOVA and Tukey's multiple comparison test.

(D) The mRNA expression of *Jun, Mcpt1*, and *Smad7* was assessed by RT-qPCR in BMMCs in response to 90 min of TGF-β (1 ng/mL) with pre-incubation of 60 min of SB431542 (5 μM) or DMSO control. The mRNA expression was normalized to *Actb*. Each replicate is represented by a different symbol. Three independent experiments are shown as mean + SD. *p<0.05, **p<0.01, ***p<0.001, ****p<0.0001 by two-way ANOVA and Fisher's LSD test.

Figure 5. SMAD1/5 action is limited by SMAD2.

(A) The Volcano plot shows the distribution of differentially expressed genes in PMC-306 S2KO vs. parental cells in response to 90 min of TGF-β (1 ng/mL). The x-axis represents the log2 fold change, while the y-axis shows the adjusted p-value. Selected genes of interest are indicated in red.

(B, *upper*) The mRNA expression of *Id2* was evaluated by RT-qPCR in resting PMC-306 parental and S2KO cells. The mRNA expression was normalized to *Actb*. Each replicate is represented by a different symbol. Three independent experiments are shown as mean + SD. *p<0.05 by unpaired t-test. (B, *lower*) Expression of ID2 protein in extracts from resting

PMC-306 parental and S2KO cells was analyzed by Western Blot. β-Actin served as loading control.

(C) Differentially expressed genes from PMC-306 parental and S2KO cells in response to 90 min of Ag (2 ng/mL), TGF-β (1 ng/mL), and Ag + TGF-β. Floating bars display the normalized read counts of *Id2* and *Id3* (NGS analysis). Each replicate is represented by a different symbol. *p<0.05, **p<0.01, ***p<0.001, ****p<0.0001 by two-way ANOVA and Tukey's multiple comparison test.

(D) The mRNA expression of *Id2* and *Id3* was assessed by RT-qPCR in PMC-306 parental and S2KO cells (*upper row*) and BMMCs (*lower row*) in response to 90 min of TGF-β (1 ng/mL) with pre-incubation of 60 min SB431542 (5 μM) or DMSO control. The mRNA expression was normalized to *Actb*. Each replicate is represented by a different symbol. Three independent experiments are shown as mean + SD. *p<0.05, **p<0.01, ***p<0.001, ****p<0.0001 by two-way ANOVA and Tukey's multiple comparison test (*upper row*) or Fisher's LSD test (*lower row*).

(E) Representative Western blot analysis of P-SMAD1/5-CT (S463/465), ID2, SMAD1, TβRII, P-SMAD2-CT (S465/467), SMAD2, and MCPT1 in protein extracts from PMC-306 parental and S2KO cells in response to 30 min (*left*) or 24 h (*right*) TGF-β (1 ng/mL) with pre-incubation of 60 min SB431542 (5 μM) or DMSO control. Asterisks indicate detection on the same membrane.

(F) Representative Western blots for P-SMAD1/5-CT and SMAD2 analysis in protein extracts from PMC-306 parental and S2KO cells in response to 60 min of TGF-β (1 ng/mL) or BMP-2 (50 ng/mL) with pre-incubation of 60 min SB431542 (5 μM), LDN193189 (5 μM) or DMSO control. Asterisks indicate detection on the same membrane. β-Actin served as a loading control.

(G) The mRNA expression of *Id2* and *Id3* was assessed by RT-qPCR in PMC-306 parental and S2KO cells in response to 60 min of TGF-β (1 ng/mL) or BMP-2 (50 ng/mL) with pre-incubation of 60 min LDN193189 (10 μM) or DMSO control. The mRNA expression was

normalized to *Actb*. Each replicate is represented by a different symbol. Three independent experiments are shown as mean + SD. *p<0.05, **p<0.01, ***p<0.001, ****p<0.0001 by two-way ANOVA and Tukey's multiple comparison test.

Figure 6. SMAD2 acts as a signaling hub in FcεRI-triggered MCs.

(A) The Volcano plot shows the distribution of differentially expressed genes in PMC-306 parental vs. S2KO cells in response to 90 min of Ag (2 ng/mL). The x-axis represents the log2 fold change, while the y-axis shows the adjusted p-value. Selected genes of interest are indicated.

(B) The mRNA expression of *Il6* and *Tnf* was assessed by RT-qPCR in PMC-306 parental and S2KO cells in response to 90 min of Ag (2 ng/mL). The mRNA expression was normalized to *Gapdh*. Each replicate is denoted by a different symbol. Three independent experiments are presented as mean + SD. *p<0.05, **p<0.01, ***p<0.001, ****p<0.0001 by two-way ANOVA and Fisher's LSD test.

(C) The secretion of IL-6 and TNF from PMC-306 parental and S2KO cells in response to 3 h of Ag (2 and 20 ng/mL) was measured by ELISA. Each replicate is denoted by a different symbol. Three independent experiments are shown as mean + SD. *p<0.05, **p<0.01, ***p<0.001, ****p<0.0001 by two-way ANOVA and Tukey's multiple comparison test.

(D) The mRNA expression of *Il6* and *Tnf* was assessed by RT-qPCR in PMC-306 parental and S2KO cells in response to Ag (2 ng/mL) for the indicated time points. The mRNA expression was normalized to *Gapdh*. Each replicate is denoted by a different symbol. Three independent experiments are presented as log2FC.

(E) The secretion of IL-6 and TNF from PMC-306 parental and S2KO cells in response to Ag (2 ng/mL) for the indicated time points was measured by ELISA. Each replicate is denoted by a different symbol. Three independent experiments are shown.

(F) The mRNA expression of *Tnf* and *Il13* was assessed by RT-qPCR in BMMCs in response to 90 min of Ag (20 ng/mL) with pre-incubation of 30 min CHX (10 µg/ml) or DMSO control. The mRNA expression was normalized to *Gapdh*. Each replicate is denoted by a different

symbol. Three independent experiments are presented as mean + SD. *p<0.05, **p<0.01, ***p<0.001 by one-way ANOVA and Tukey's multiple comparison test.

(G) The mRNA expression of *Tnf* and *Il13* was assessed by RT-qPCR in PMC-306 parental and S2KO cells in response to 90 min of Ag (2 ng/mL) with pre-incubation of 30 min CHX (10 µg/mL) or DMSO control. The mRNA expression was normalized to *Gapdh*. Each replicate is denoted by a different symbol. Three independent experiments are presented as mean + SD. *p<0.05, **p<0.01, ***p<0.001 by two-way ANOVA and Tukey's multiple comparison test.

Figure 7. Ag- and TGF-β-induced MC activation exhibit differential sensitivity to SMAD2 expression levels.

(A,B) Representative Western blots for P-SMAD2-CT (S465/467), P-SMAD2-L (S245/250/255), SMAD2 and V5 as analyzed in protein extracts prepared from PMC-306 parental (transfected with empty vector; EV), S2KO cells (transfected with empty vector; KO EV), and S2KO cells transfected with 3xV5-Smad2 (V5S2) in response to 15 min Ag (2 ng/mL) (A) and 15 min TGF-β (1 ng/mL) (B). GAPDH served as the loading control. Asterisks indicate detection on the same membrane.

(C) The mRNA expression of *Smad2* was assessed by RT-qPCR in PMC-306 parental EV, KO EV and KO V5S2 cells in response to 90 min TGF-β (1 ng/mL). The mRNA expression was normalized to *Actb*. Each replicate is represented by a different symbol. Three independent experiments are shown as mean + SD. *p<0.05, **p<0.01, ***p<0.001 by two-way ANOVA and Tukey's multiple comparison test.

(D-F) The mRNA expression of *Il6* (D), *Tnf* (E), and *Il13* (F) were assessed by RT-qPCR in PMC-306 parental EV, KO EV and KO V5S2 cells in response to 90 min Ag (2 ng/mL). The mRNA expression was normalized to *Gapdh*. Each replicate is represented by a different symbol. Three independent experiments are shown as mean + SD. *p<0.05, **p<0.01, ***p<0.001 by two-way ANOVA and Tukey's multiple comparison test.

(G,H) The secretion of IL-6 (G) and TNF (H) from PMC-306 parental EV, KO EV and KO V5S2 cells in response to 3 h Ag (2 ng/mL) was measured by ELISA. Each replicate is represented

by a different symbol. Three independent experiments are shown as mean + SD. *p<0.05, **p<0.01, ***p<0.001 by two-way ANOVA and Tukey's multiple comparison test.

(I, J) The mRNA expression of *Jun* (I) and *Smad7* (J), were assessed by RT-qPCR in PMC-306 parental EV, KO EV and KO V5S2 cells in response to 90 min TGF-β (1 ng/mL). The mRNA expression was normalized to *Actb*. Each replicate is represented by a different symbol. Three independent experiments are shown as mean + SD. *p<0.05, **p<0.01, ***p<0.001, ****p<0.0001 by two-way ANOVA and Tukey's multiple comparison test.

(K, L) Western blots for P-SMAD2-CT, P-SMAD1/5-CT (S463/465), SMAD2, JUN and MCPT1 of protein extracts from PMC-306 parental EV, KO EV and KO V5S2 cells in response to 1 h (K) or 24 h (L) TGF-β (1 ng/mL). HSP90 served as loading control. Asterisks indicate detection on the same membrane.

(M, N) The mRNA expression of *Id2* (M) and *Id3* (N) were assessed by RT-qPCR in PMC-306 parental EV, KO EV and KO V5S2 cells in response to 90 min TGF-β (1 ng/mL). The mRNA expression was normalized to *Actb*. Each replicate is represented by a different symbol. Three independent experiments are shown as mean + SD. *p<0.05, **p<0.01, ***p<0.001, ****p<0.0001 by two-way ANOVA and Tukey's multiple comparison test.

Supplemental Figure 1.

(A-C) Representative Western blots for P-SMAD2-CT (S465/467), P-SMAD2-L (S245/250/255), SMAD2, and P-ERK1/2 (T202/Y204) in protein extracts from BMMCs in response to Ag (20 ng/mL) and TGF-β (1 ng/mL) for the indicated time points. HSP90 served as loading control. Asterisks indicate detection on the same membrane. (B, C) Quantitative analysis of P-SMAD2-CT and P-SMAD2-L levels relative to HSP90 from three independent experiments are shown as mean + SD. *p<0.05, **p<0.01 by one-way ANOVA and Dunnett's multiple comparison test.

(D-F) Representative Western blots for P-SMAD2-CT, P-SMAD2-L, and SMAD2 in protein extracts from BMMCs in response to 5 and 15 min TGF-β (1 ng/mL) with pre-incubation of 30 min SB431542 (5 μM) or DMSO control. HSP90 served as the loading control. Asterisks indicate detection on the same membrane. (E, F) Quantitative analysis of P-SMAD2-CT and P-SMAD2-L levels relative to HSP90 from three independent experiments are shown as mean + SD. *p<0.05, **p<0.01 by one-way ANOVA and Tukey's multiple comparison test.

(G-I) Representative Western blots for P-SMAD2-CT, P-SMAD2-L, and P-ERK1/2 in protein extracts from PMC-306 cells in response to 15 min TGF-β (1 ng/mL), 15 min Ag (2 ng/mL), and 15 min SCF (30 ng/mL) with pre-incubation of 30 min Trametinib (50 nM) or DMSO control. HSP90 served as loading control. Asterisks indicate detection on the same membrane. Non-relevant lanes were removed from the blot. The removal is indicated by a dashed line.

(H, I) Quantitative analysis of P-SMAD2-CT and P-SMAD2-L levels relative to HSP90 from three independent experiments are shown as mean + SD. *p<0.05, **p<0.01, ***p<0.001, ****p<0.0001 by two-way ANOVA and Tukey's multiple comparison test.

Supplemental Figure 2.

(A) The Volcano plots show the distribution of differentially expressed genes in BMMCs in response to TGF-β (1 ng/mL; *left panel*), Ag (20 ng/mL; *middle panel*) and Ag + TGF-β (*right*

panel) for 90 min. The x-axis represents the log2 fold change, while the y-axis shows the adjusted p-value. Selected genes of interest are indicated.

(B, C) Differentially expressed genes from BMMCs in response to Ag (20 ng/mL), TGF-β (1 ng/mL), and Ag + TGF-β for 90 min. Floating bars display the normalized read counts (NGS analysis) of *Smads* (B) and negative regulators (C). Each replicate is represented by a different symbol. *p<0.05, **p<0.01, ***p<0.001, ****p<0.0001 by one-way ANOVA and Tukey's multiple comparison test.

Supplemental Figure 3.

(A) The depicted CRISPR-Cas9 gRNA sequence (red box) against *Smad2* was used to generate PMC-306 SMAD2 KO cells.

(B, C) Multiple clones were collected from which number 10, 29 and 35 were sequenced (B) and subsequently selected for experiments. Clone 10 and 35 had the same single nucleotide insertion, while clone 29 had a 8 nucleotide deletion. Those changes result in frame shifts and cause premature stop codons (nonsense mutations) in the amino acid sequence (C, indicated with asterisks).

(D) Western blots for SMAD2 using protein extracts from PMC-306 S2parental and S2KO cells, with HSP90 serving as the loading control.

(E) Sequence alignment of *Smad2* with *Smad3*, *Smad1* and *Smad5*, respectively. The red box marks the binding site of the CRISPR-Cas9 gRNA.

Supplemental Figure 4.

Differentially expressed receptor genes from PMC-306 parental and S2KO cells in response to 90 min of Ag (2 ng/mL), TGF-β (1 ng/mL), and Ag + TGF-β. The floating bars display the normalized read counts from NGS analysis, with each replicate represented by a unique symbol. *p<0.05, **p<0.01, ***p<0.001, ****p<0.0001 by two-way ANOVA and Tukey's multiple comparison test.

Supplemental Figure 5.

(A) Differentially expressed *Smad* genes in PMC-306 parental and S2KO cells in response to 90 min Ag (2 ng/mL), TGF-β (1 ng/mL), and Ag + TGF-β. The floating bars display the normalized read counts from NGS analysis, with each replicate represented by a unique symbol. *p<0.05, **p<0.01, ***p<0.001, ****p<0.0001 by two-way ANOVA and Tukey's multiple comparison test.

(B) The expression of *Smad2*, *Smad2ΔExon3*, *Smad3*, *Smad1* and *Smad5* was assessed in resting murine primary hepatic stellate cells (mHSCs), PMC-306 parental and S2KO cells, as well as primary PMCs using RT-qPCR. *Actb* was used as the loading control.

(C) Expression of the *Skil* gene was identified in PMC-306 parental and S2KO cells in response to 90 min of Ag (2 ng/mL), TGF-β (1 ng/mL), and Ag+TGF-β. The floating bars display the normalized read counts (NGS analysis). Each replicate is represented by a different symbol. *p<0.05, **p<0.01, ***p<0.001, ****p<0.0001 by two-way ANOVA and Tukey's multiple comparison test.

Supplemental Figure 6.

(A) Differentially expressed genes (*Id2*, *Id3*, *Smad7*, *Skil*, *Nfkbia*, *Spry2*, *Sh2b2*, and *Sh2b3*) from PMC-306 parental and S2KO cells in response to 20 and 90 min of TGF-β (1 ng/mL). The floating bars display the normalized read counts from NGS analysis. Each replicate is represented by a different symbol. *p<0.05, **p<0.01, ***p<0.001, ****p<0.0001 by two-way ANOVA and Tukey's multiple comparison test.

(B) Differentially expressed genes (*Id2*, *Id3*, *Smad7*, *Skil*, *Nfkbia*, *Spry2*, *Sh2b2*, and *Sh2b3*) from BMMCs in response to 90 min of TGF-β (1 ng/mL) stimulation. The floating bars display the normalized read counts from NGS analysis. Each replicate is represented by a different symbol. *p<0.05, **p<0.01, ***p<0.001, ****p<0.0001 by unpaired t-test.

Supplemental Figure 7.

(A, B) The mRNA expression of *Il6* and *Tnf* was assessed by RT-qPCR in PMC-306 parental and S2KO cells in response to either 15 min (A) or the indicated time points (B) of Ag (2 ng/mL). The mRNA expression was normalized to *Gapdh*. Each replicate is represented by a different symbol. Three independent experiments are shown as mean + SD. *p<0.05 by two-way ANOVA and Fisher's LSD test (A) or as mean + SD. *p<0.05, **p<0.01, ***p<0.001 by two-way ANOVA and Tukey's multiple comparison test (B).

(C) The secretion of IL-6 and TNF from PMC-306 parental and S2KO cells in response to Ag (2 ng/mL) for the indicated time points was measured by ELISA. Each replicate is represented by a different symbol. Three independent experiments are shown as mean + SD. *p<0.05, **p<0.01, ***p<0.001, ****p<0.0001 by two-way ANOVA and Tukey's multiple comparison test.

(D) Differentially expressed NFκB target genes (*Il1b*, *Nfkbia*, *Nfkb1*, *Tnfaip3*, and *Nlrp3*) from PMC-306 parental and S2KO cells in response to 20 and 90 min of Ag (2 ng/mL). Floating bars display the normalized read counts (NGS analysis). Each replicate is represented by a different symbol. *p<0.05, **p<0.01, ***p<0.001, ****p<0.0001 by two-way ANOVA and Tukey's multiple comparison test.

Supplemental Figure 8.

(A) Representative Western blots for SMAD2 and V5-tag in protein extracts from single-colony PMC-306 parental empty vector (EV), S2KO EV and S2KO 3xV5-Smad2 (V5S2) cells. HSP90 served as loading control. Asterisks indicate detection on the same membrane.

(B) The mRNA expression of *Id1* was evaluated by RT-qPCR in PMC-306 parental EV, S2KO EV, and S2KO V5S2 cells after 90 min of TGF-β (1 ng/mL) treatment. The mRNA expression was normalized to *Actb*. Each replicate is represented by a different symbol. Three independent experiments are presented as mean + SD. *p<0.05, **p<0.01, ***p<0.001, ****p<0.0001 by two-way ANOVA and Tukey's multiple comparison test.

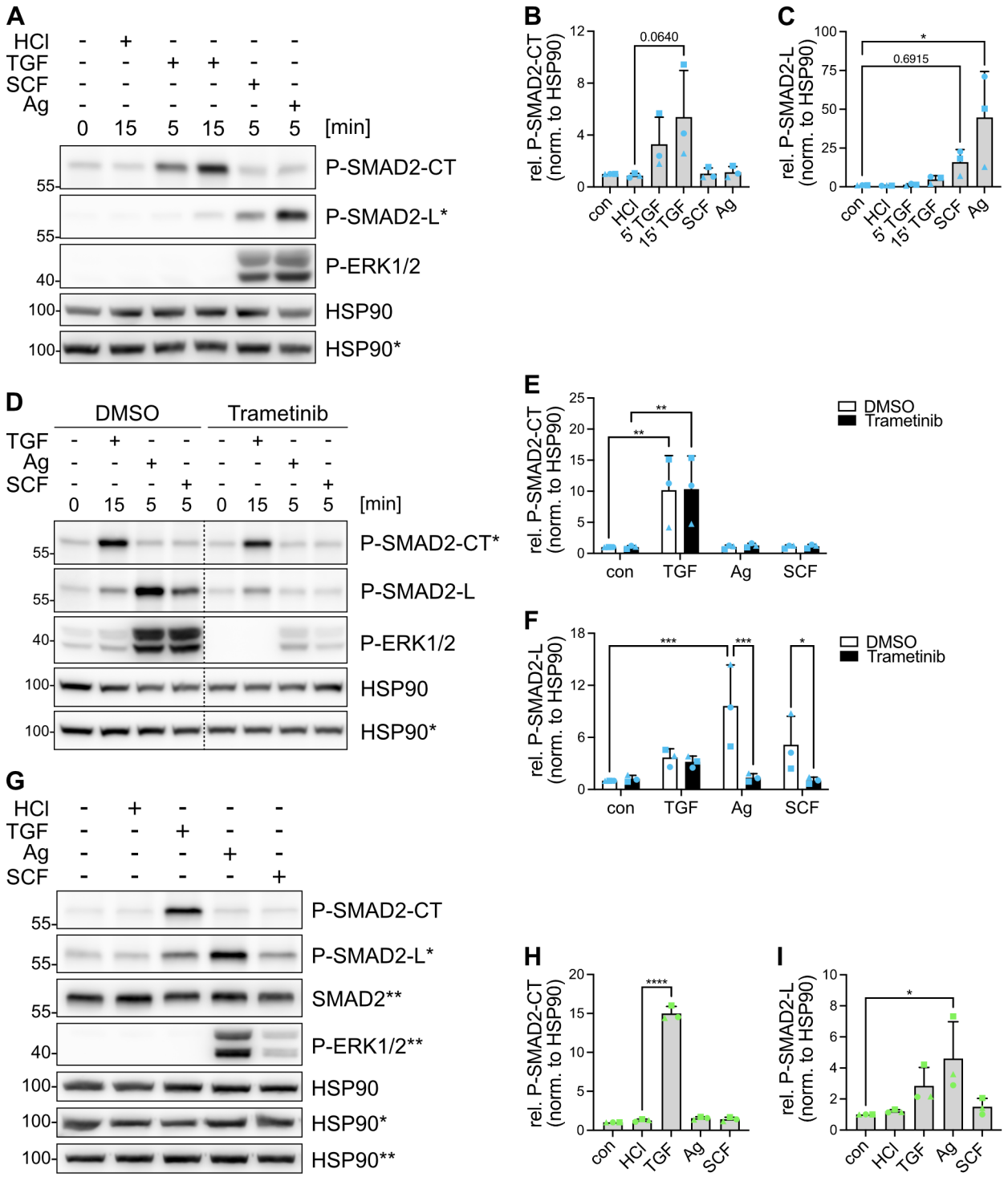

Bronneberg et al. - Fig. 1

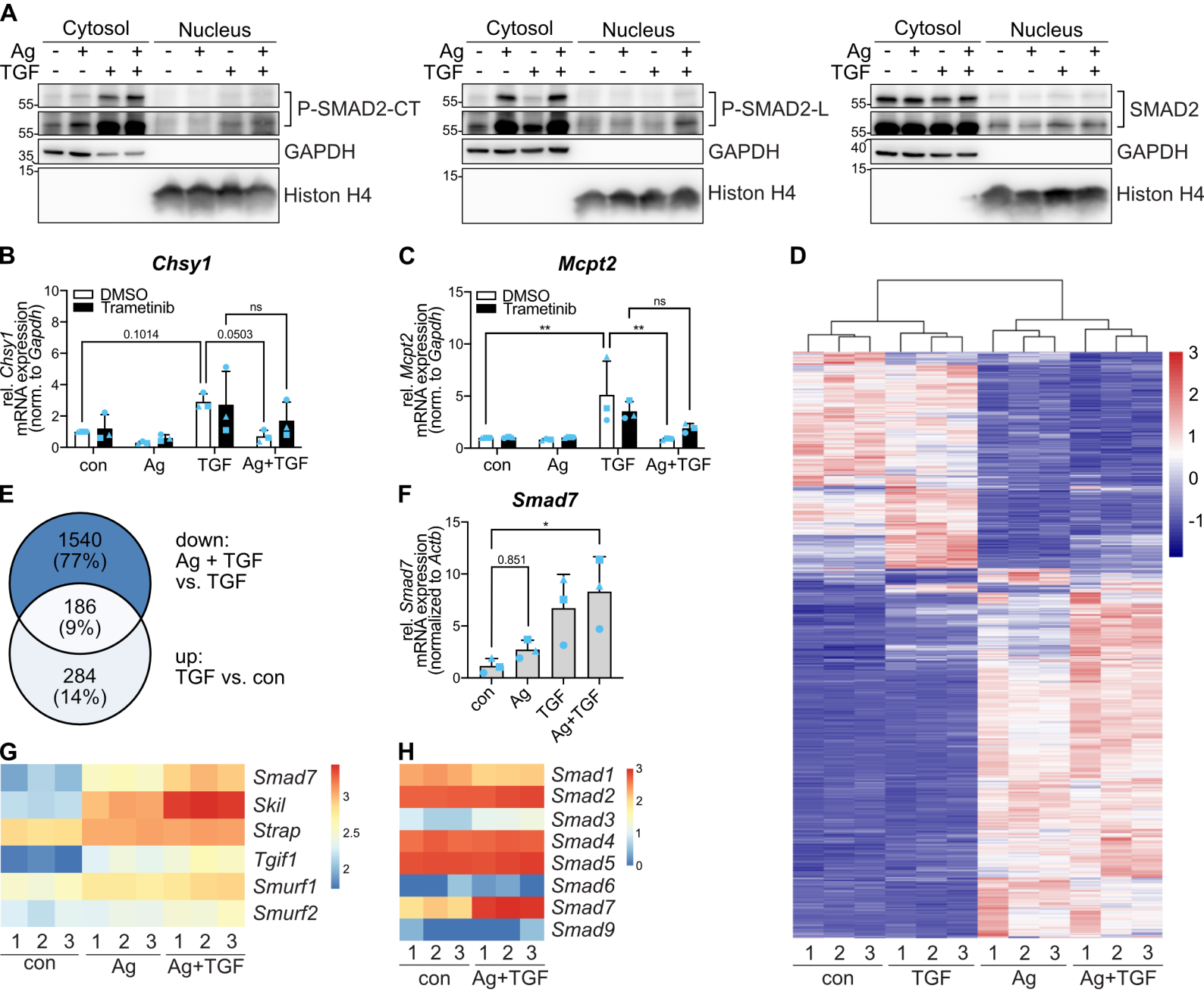

Bronneberg et al. - Fig. 2

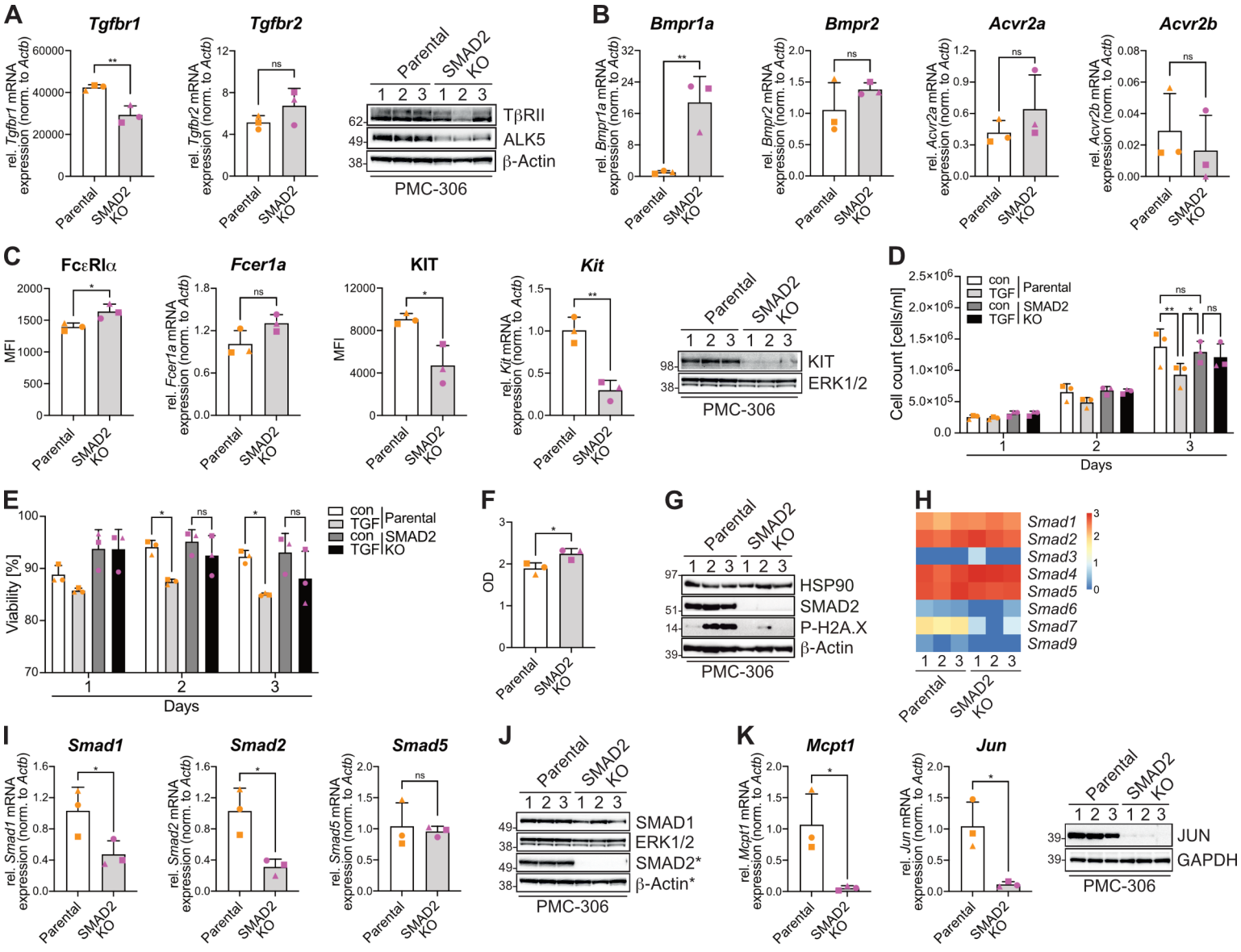

Bronneberg et al. - Fig. 3

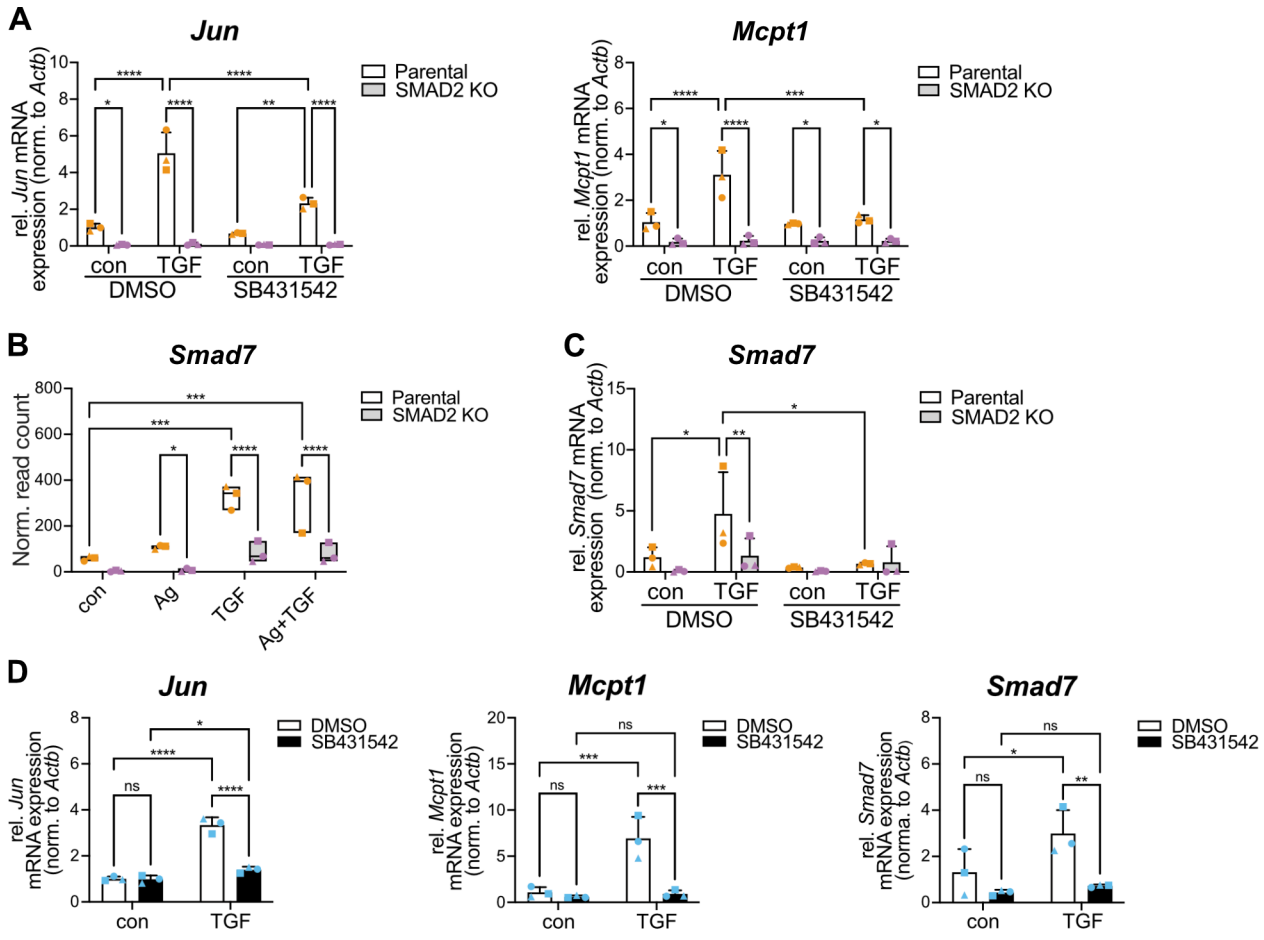

Bronneberg et al. - Fig. 4

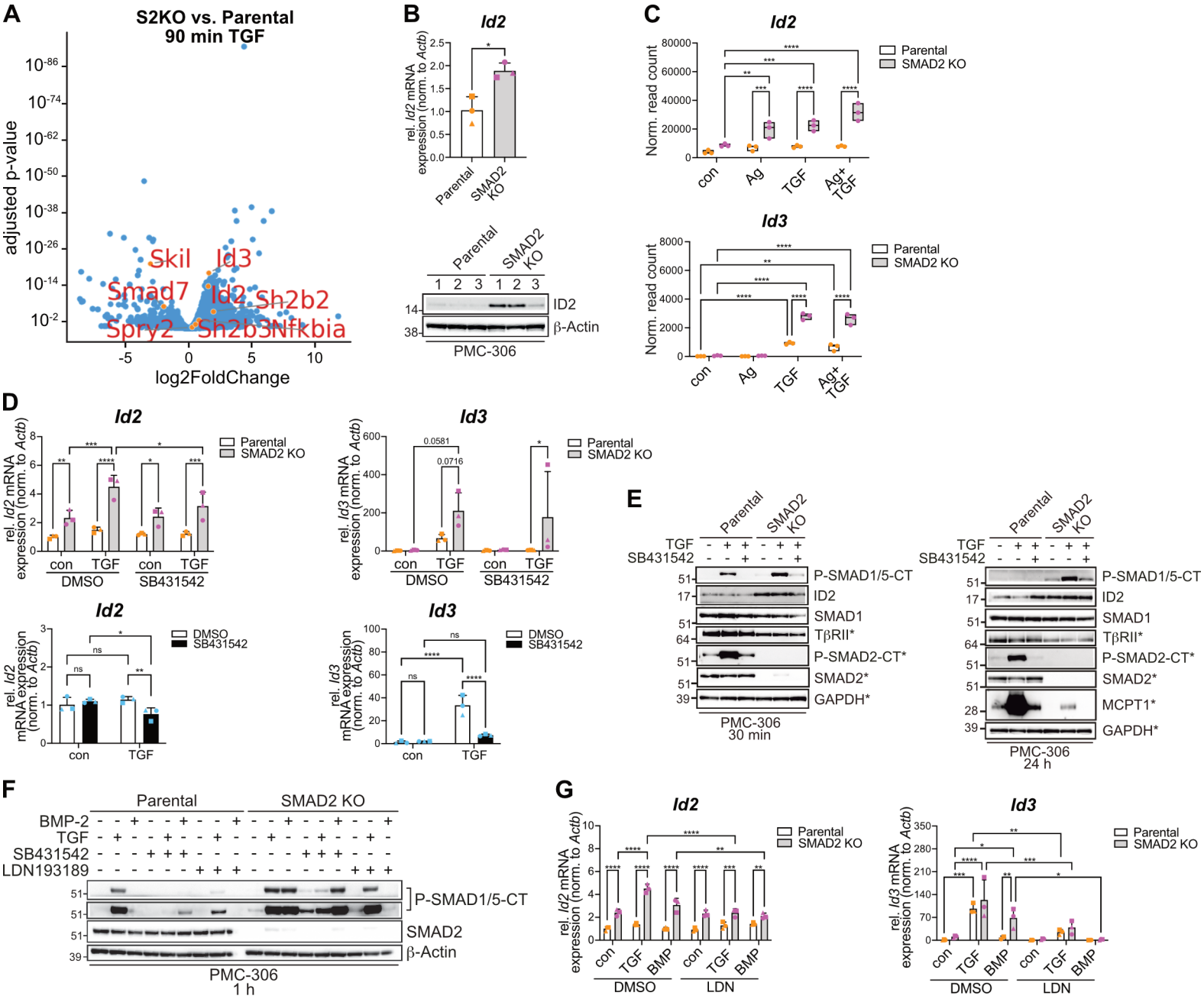

Bronneberg et al. - Fig. 5

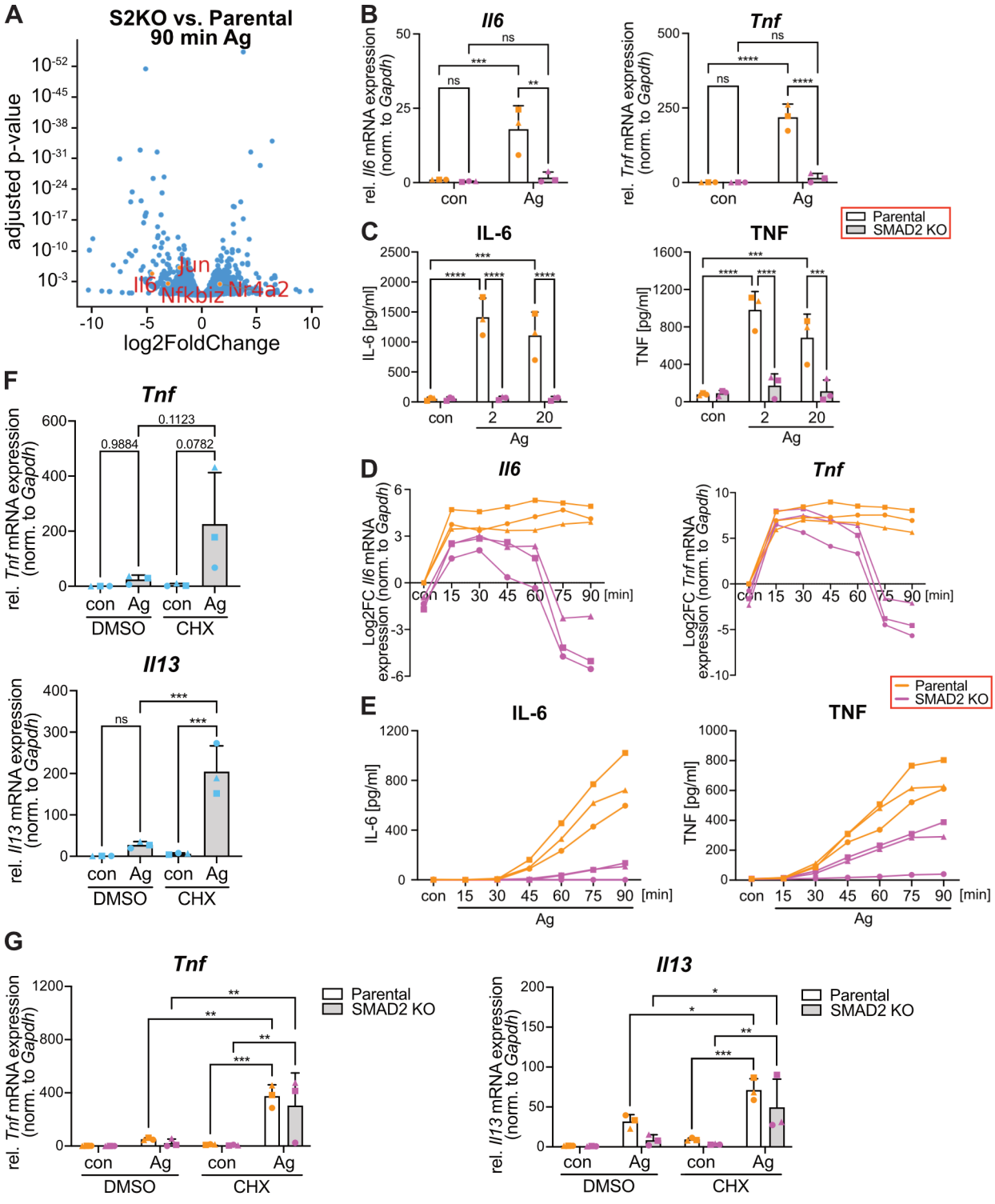

Bronneberg et al. - Fig. 6

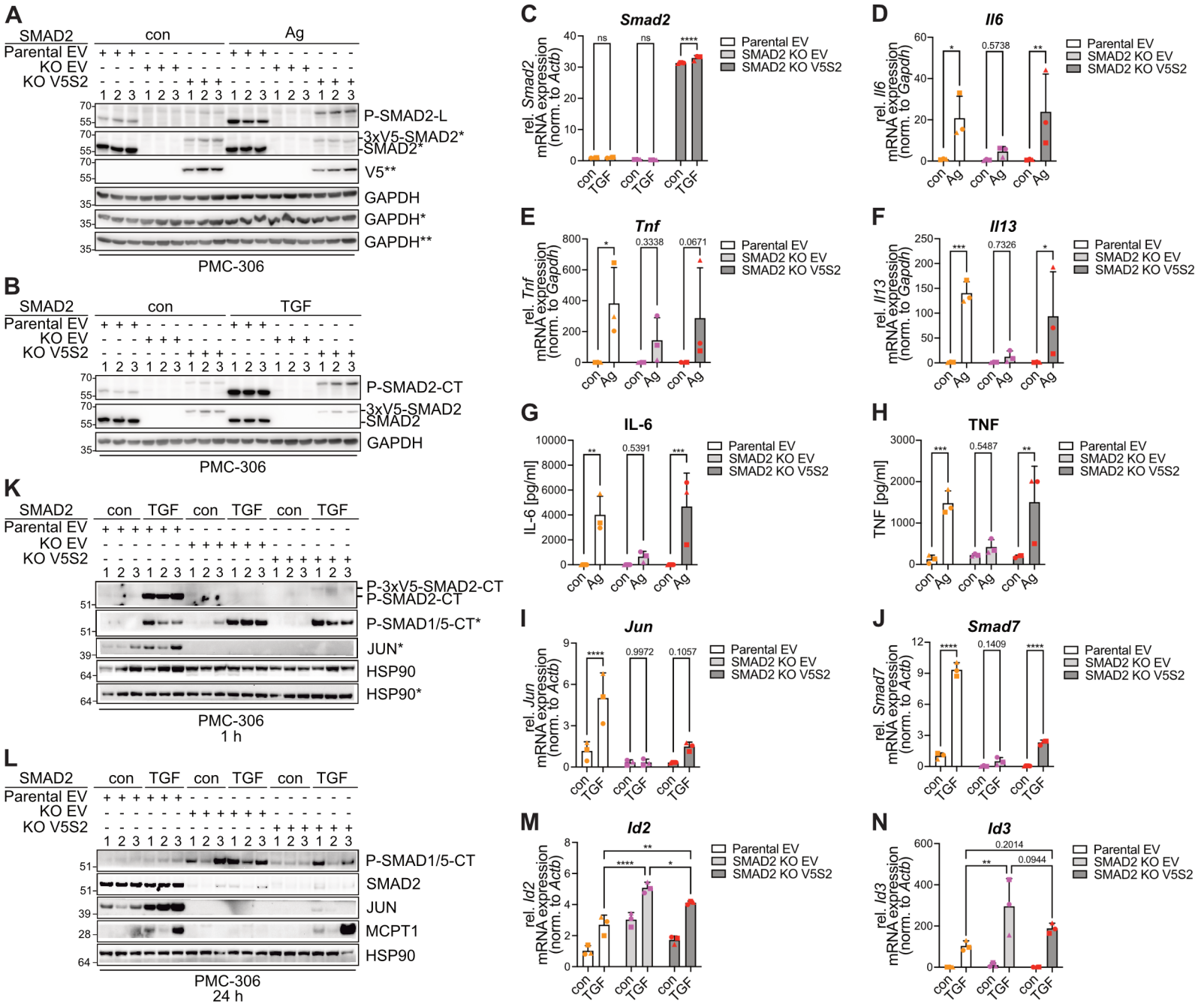

Bronneberg et al. - Fig. 7

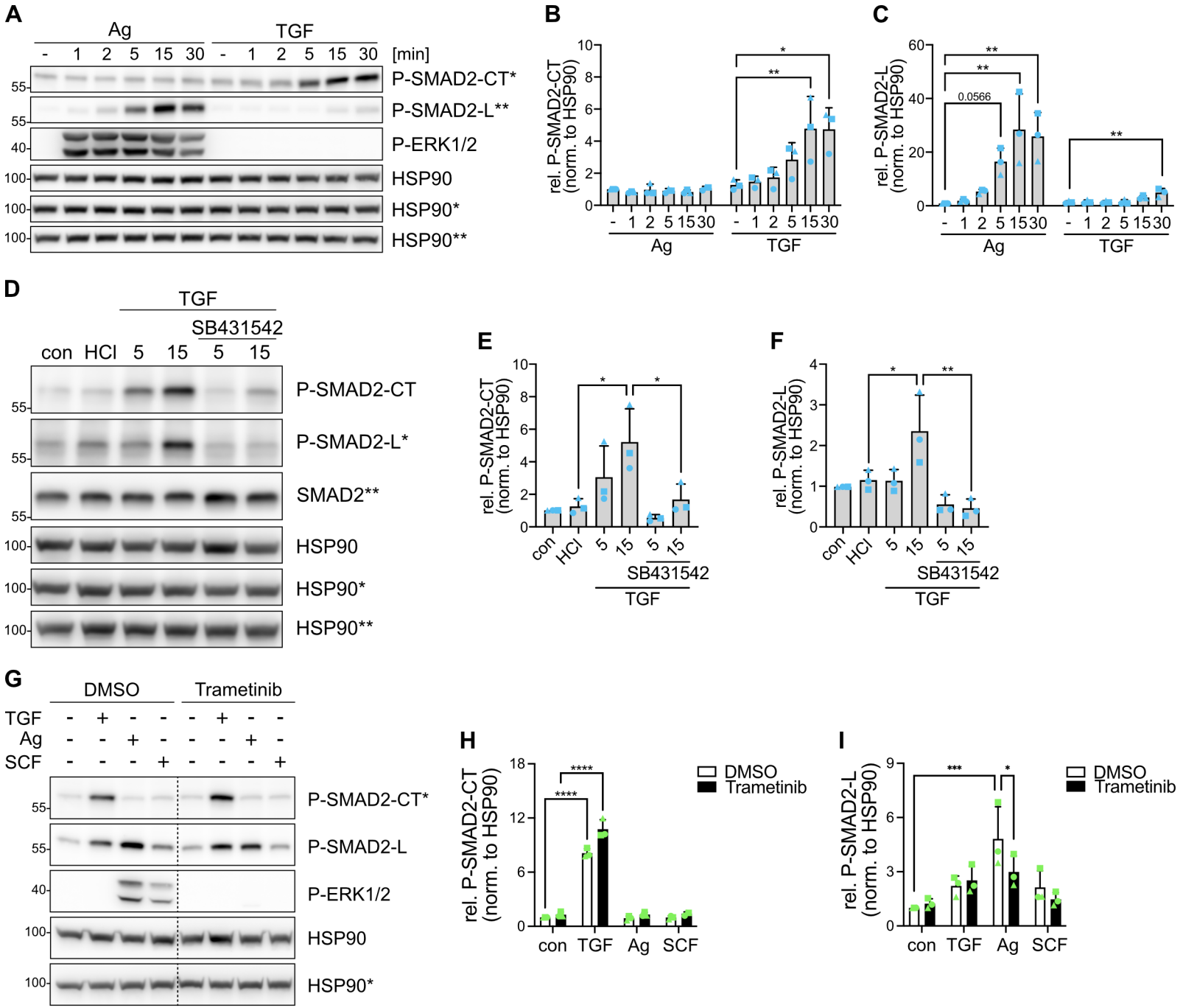

Bronneberg et al. - Suppl. Fig. 1

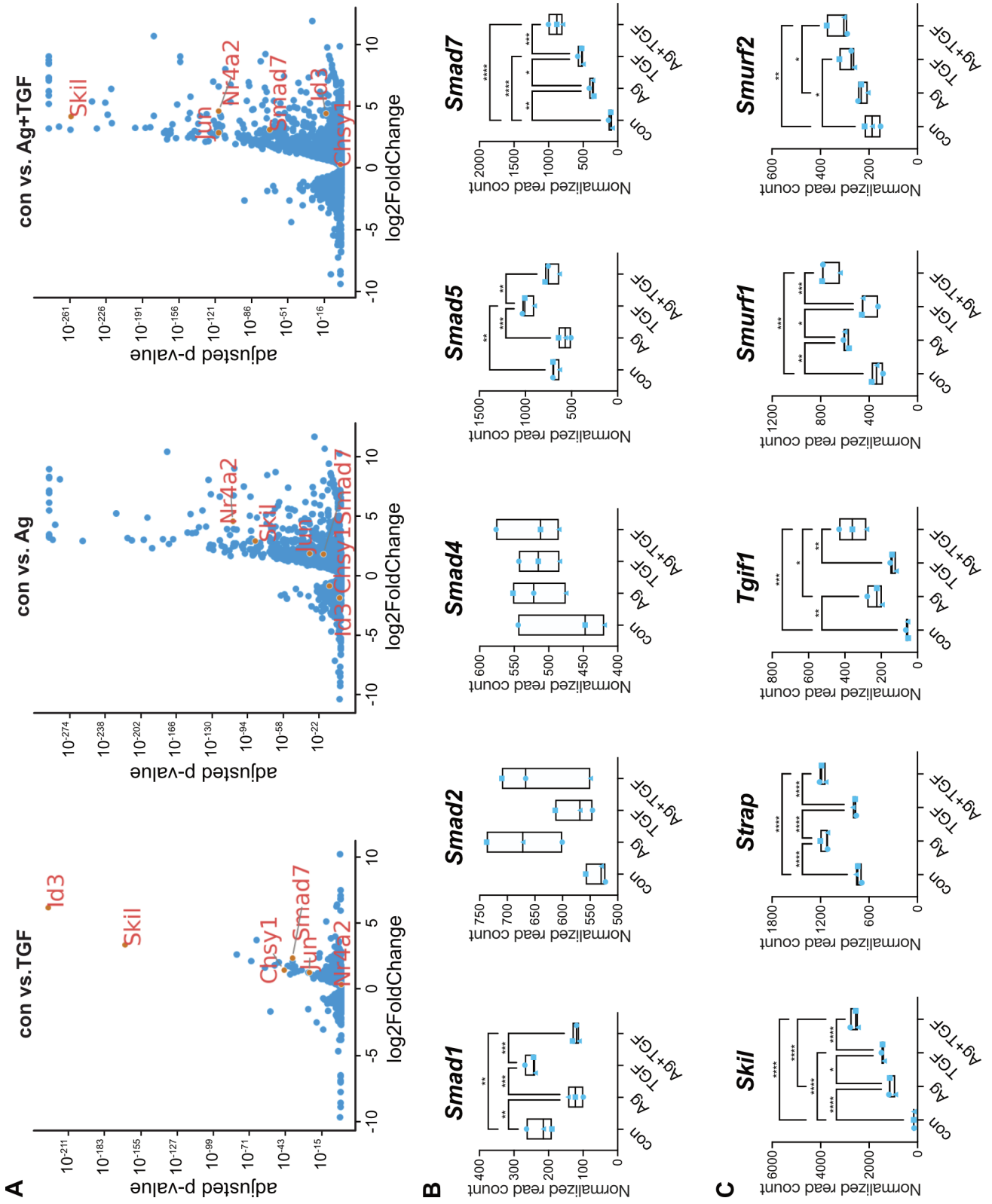

Bronneberg et al. - Suppl. Fig. 2

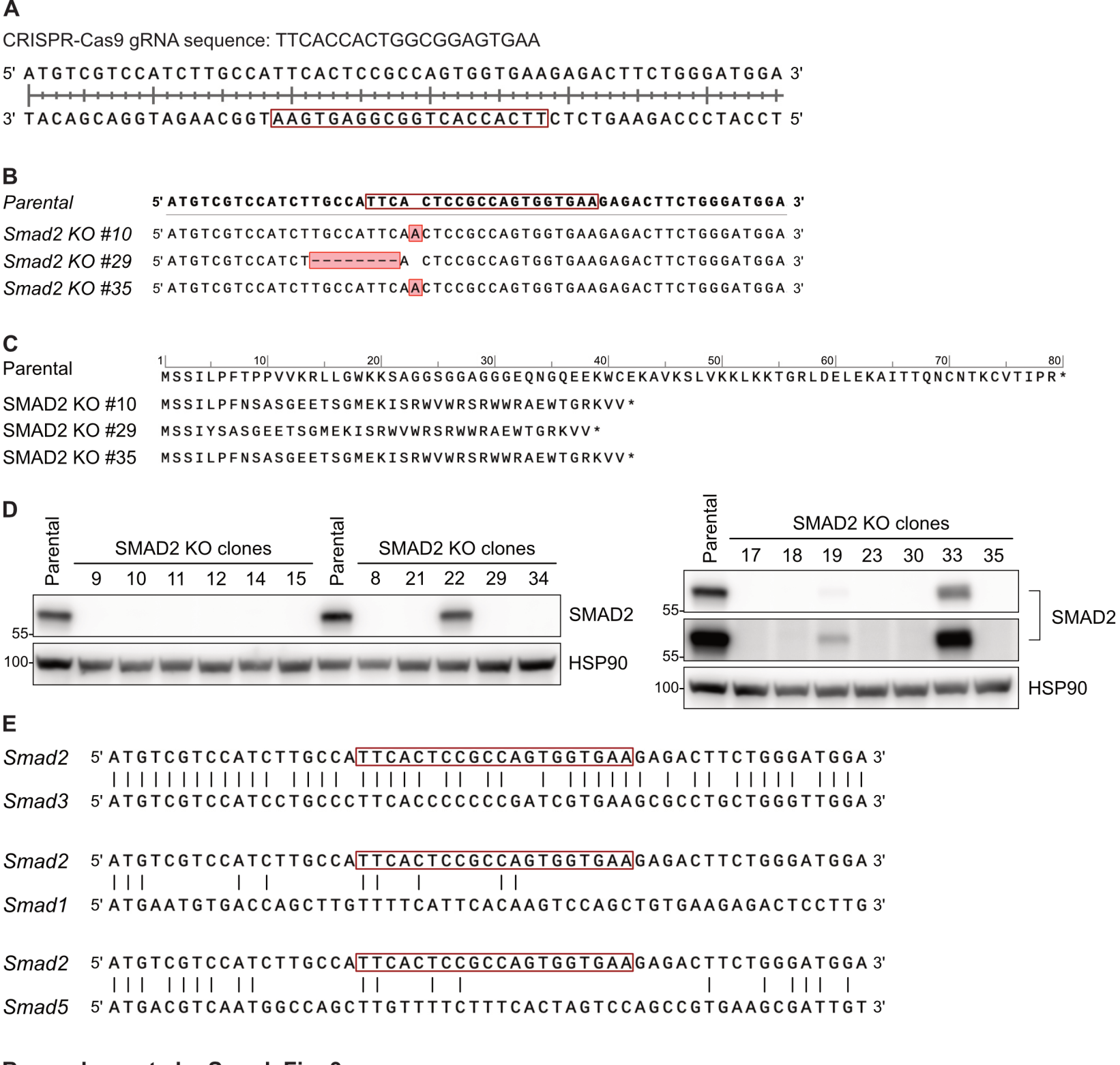

Bronneberg et al. - Suppl. Fig. 3

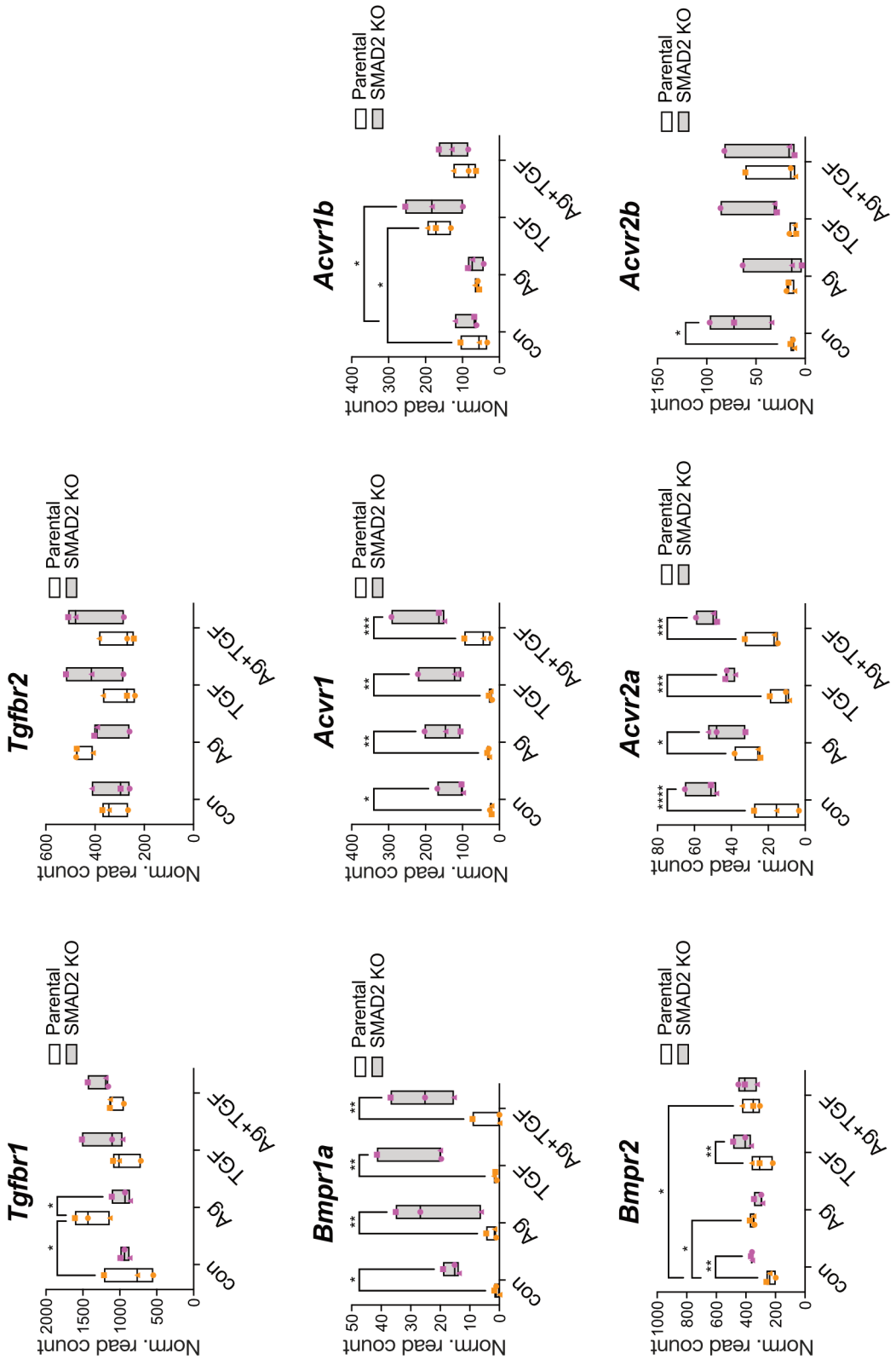

Bronneberg et al. - Suppl. Fig. 4

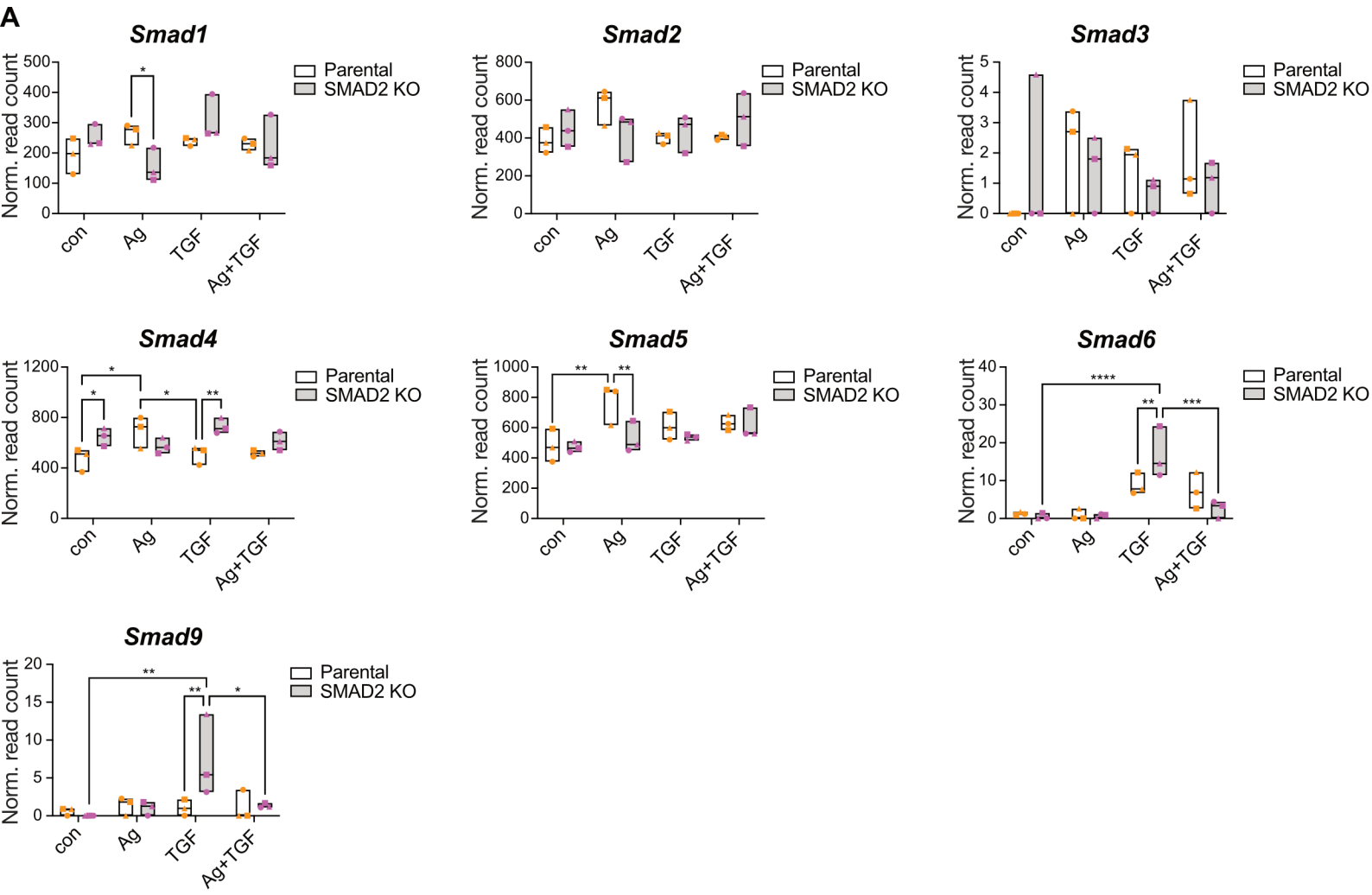

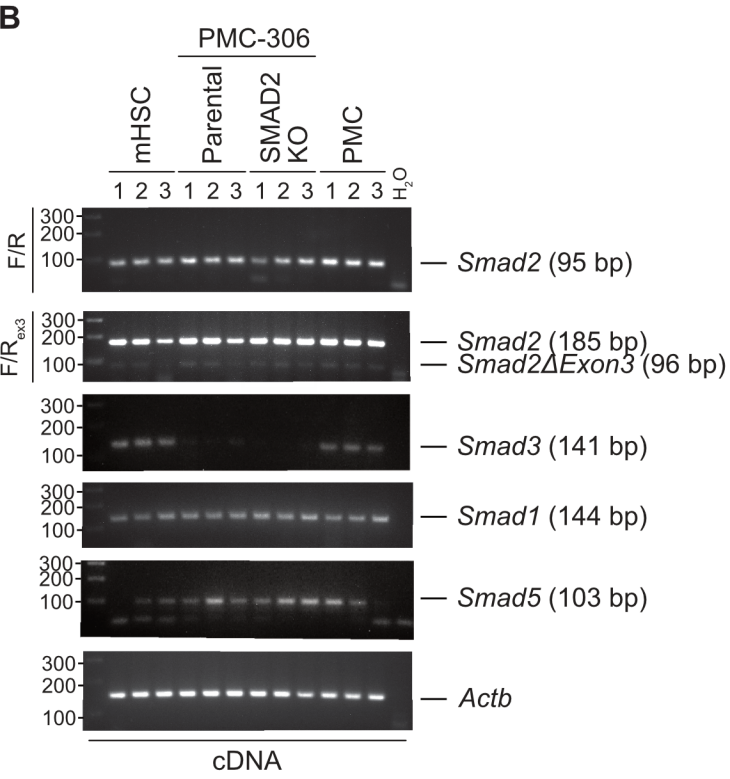

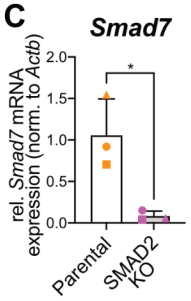

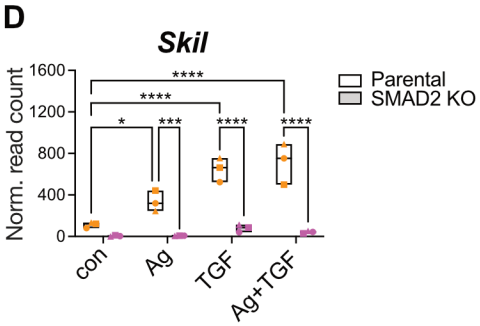

Bronneberg et al. - Suppl. Fig. 5

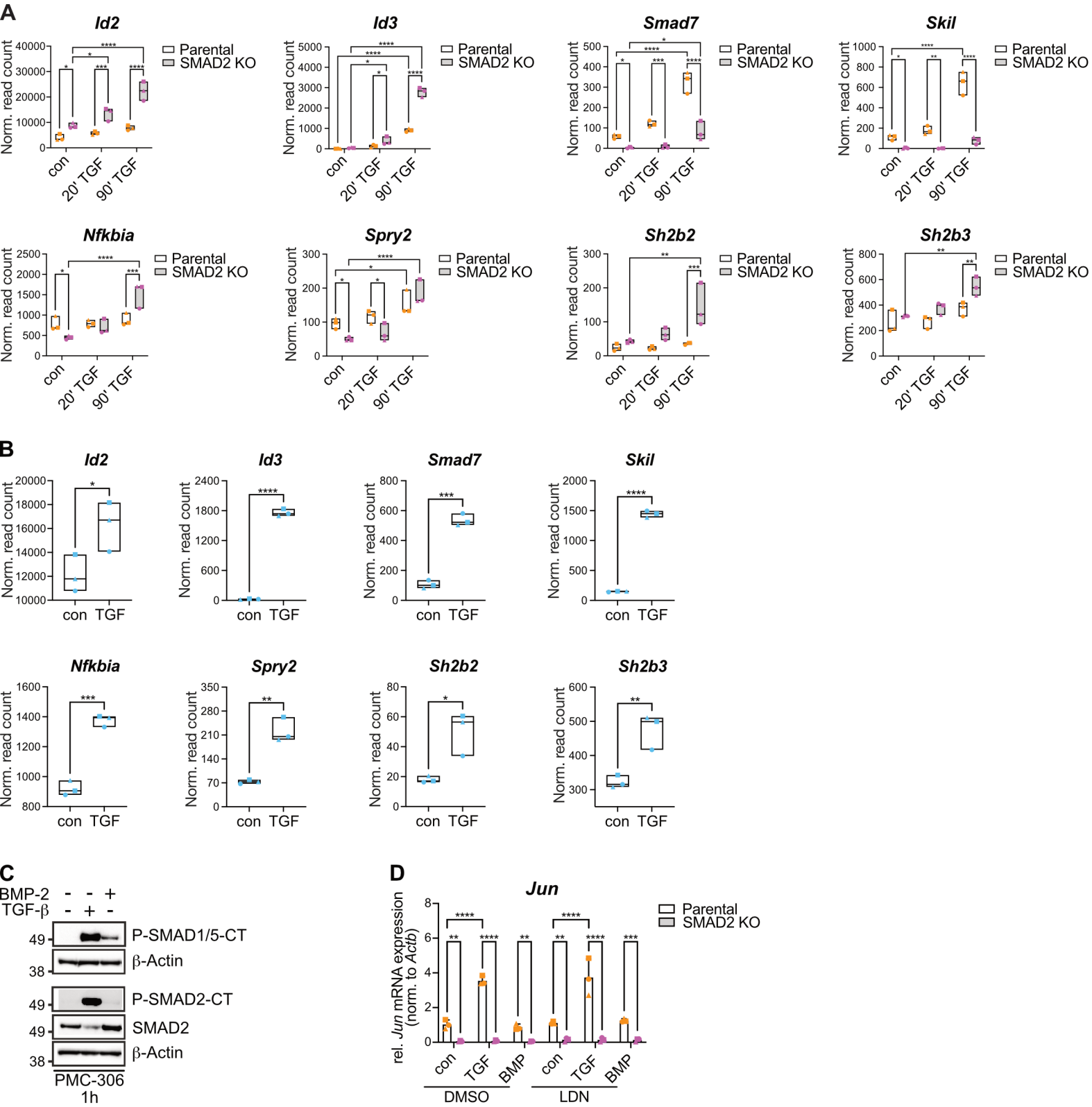

Bronneberg et al. - Suppl. Fig. 6

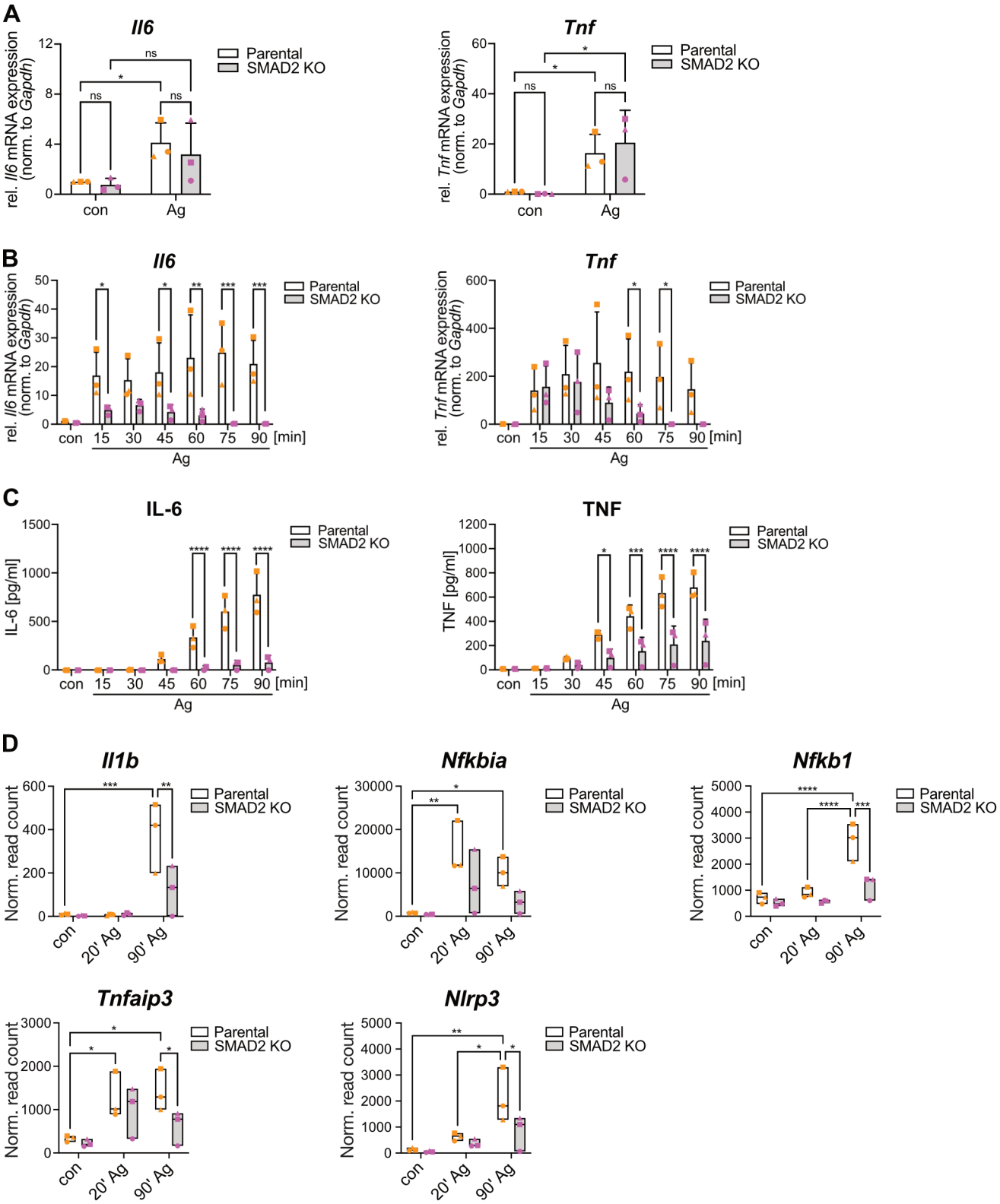

Bronneberg et al. - Suppl. Fig. 7

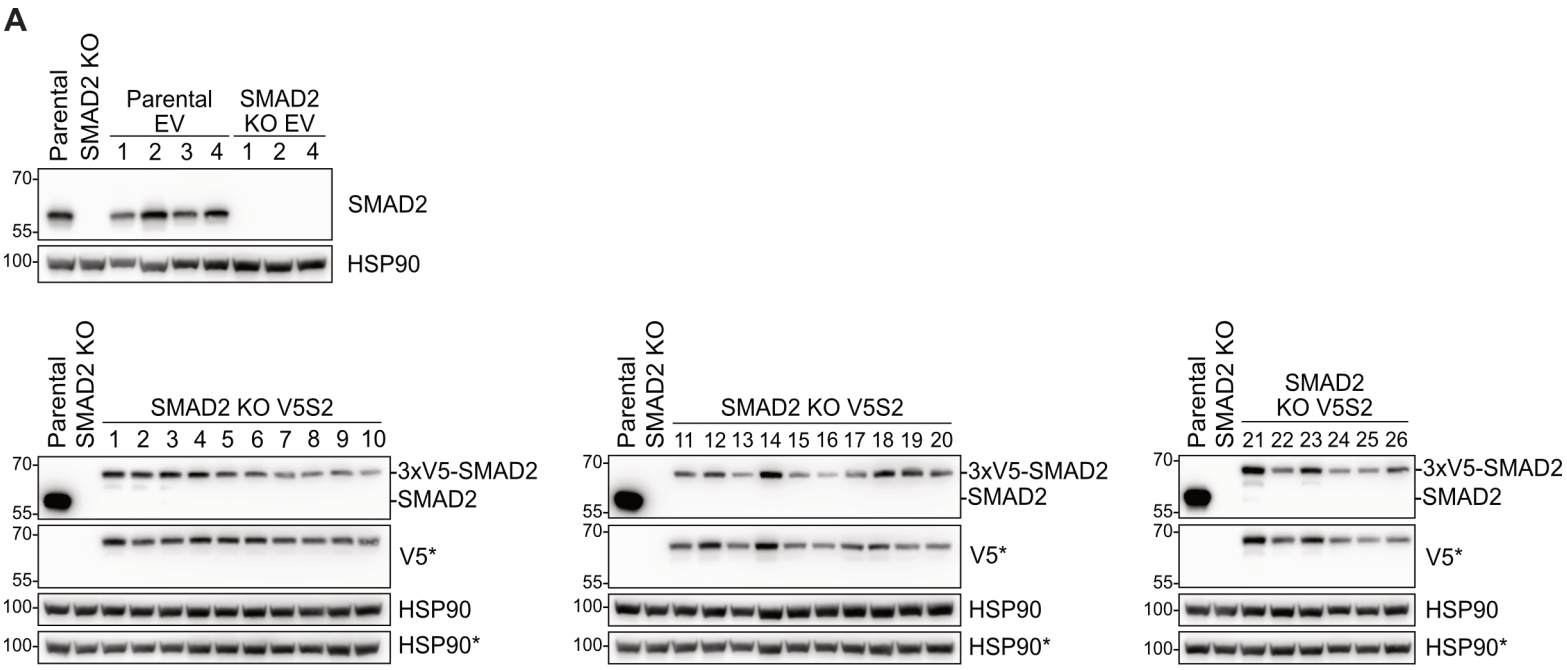

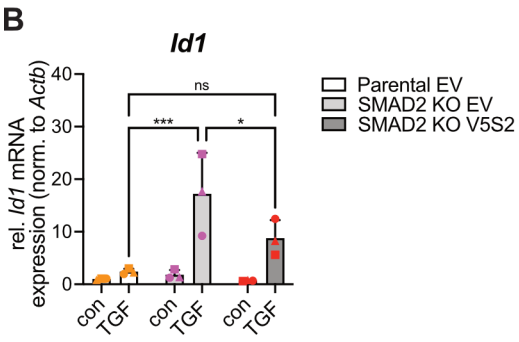

Bronneberg et al. - Suppl. Fig. 8